Published in final edited form as:

Cell Host Microbe. 2018 May 09; 23(5): 594–606.e7. doi:10.1016/j.chom.2018.04.001.

Host Nitric Oxide Disrupts Microbial Cell-to-Cell Communication to Inhibit Staphylococcal Virulence

Rodolfo Urbano[1], **Joyce E. Karlinsey**[1], **Stephen J. Libby**[2], **Paschalis-Thomas Doulias**[3,4], **Harry Ischiropoulos**[3,4], **Helen I. Warheit-Niemi**[1], **Denny H. Liggitt**[5], **Alexander R. Horswill**[6], and **Ferric C. Fang**[1,2,7,*]

[1]Department of Microbiology, University of Washington, Seattle, WA 98195, USA

[2]Department of Laboratory Medicine, University of Washington, Seattle, WA 98195, USA

[3]Children's Hospital of Philadelphia Research Institute, Philadelphia, PA 19104, USA

[4]Department of Pharmacology, University of Pennsylvania, Philadelphia, PA 19104, USA

[5]Department of Comparative Medicine, University of Washington, Seattle, WA 98195, USA

[6]Department of Immunology and Microbiology, University of Colorado Anschutz Medical Campus, Aurora, CO 80045, USA

SUMMARY

Staphylococcus aureus is a commensal bacterium that can asymptomatically colonize its host but also causes invasive infections. Quorum sensing regulates *S. aureus* virulence and the transition from a commensal to a pathogenic organism. However, little is known about how host innate immunity affects interbacterial communication. We show that nitric oxide suppresses staphylococcal virulence by targeting the Agr quorum sensing system. Nitric oxide-mediated inhibition occurs through direct modification of cysteine residues C55, C123, and C199 of the AgrA transcription factor. Cysteine modification decreases AgrA promoter occupancy as well as transcription of the *agr* operon and quorum sensing-activated toxin genes. In a staphylococcal pneumonia model, mice lacking inducible nitric oxide synthase develop more severe disease with heightened mortality and pro-inflammatory cytokine responses. Additionally, staphylococcal α-toxin production increases in the absence of nitric oxide or nitric oxide-sensitive AgrA cysteine

*Correspondence: fcfang@u.washington.edu.
[7]Lead Contact

AUTHOR CONTRIBUTIONS

R.U. performed biotin-switch assays, RT-qPCR, western blots, ChIP-qPCR, animal infections, cytokine measurements, α-toxin ELISA, and assisted J.E.K. with MRC sample preparation. S.J.L. contributed to animal experiments and collected mouse serum. P.T.D and H.I. prepared MRC resin and performed LC-MS/MS peptide analysis. H.I.W. contributed to RT-qPCR measurements. D.H.L. performed histopathological scoring. A.R.H. assisted with study design and provided reagents. R.U. and F.C.F. designed experiments, analyzed results, and wrote the manuscript.

DECLARATION OF INTERESTS

The authors declare no competing interests.

residues. Our findings demonstrate an anti-virulence mechanism for nitric oxide in innate immunity.

In Brief

Quorum sensing regulates staphylococcal virulence and mediates the transition of *S. aureus* from a commensal organism to a pathogen. Urbano et al. demonstrate that the innate immunity molecule nitric oxide can directly target the quorum sensing regulator AgrA to inhibit toxin production and protect the host against staphylococcal infection.

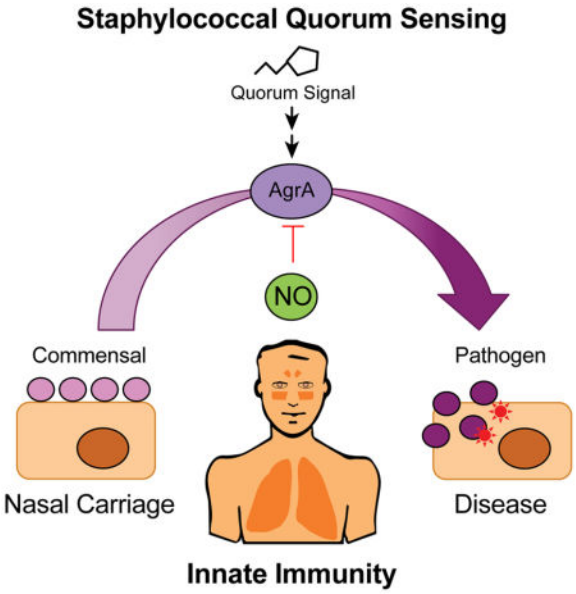

Keywords

Innate immunity; host defense; nitric oxide; *S. aureus*; virulence; bacterial pathogenesis; quorum sensing

INTRODUCTION

Nitric oxide (NO) is an important mediator of host innate immunity with antimicrobial activity against bacteria, fungi, parasites, and viruses (Fang, 1999). In the mammalian host, NO production is transcriptionally induced by upregulation of the inducible nitric oxide synthase (iNOS) enzyme in response to cytokines and microbial products (Bogdan, 2015). Macrophages and other innate immune cells expressing iNOS produce copious quantities of NO from L-arginine and molecular oxygen (MacMicking et al., 1997). The biochemical properties of NO, which include membrane permeability and targeting of intracellular protein thiols and metal centers, make NO an effective antimicrobial molecule with broad activity against diverse pathogens (Fang, 2004; Stamler et al., 2001). During infection, high cytotoxic levels of NO produced by iNOS can dramatically alter microbial metabolism and physiology. NO disruption of the electron transport chain, tricarboxylic acid cycle enzymes, and ribonucleotide reductase can impair fundamental physiological processes such as

respiration, metabolism, and DNA replication (Fang, 2004; Richardson et al., 2011). Collectively, these antimicrobial actions known as nitrosative stress benefit the host by inhibiting pathogen growth during infection.

Bacterial pathogens have evolved diverse strategies to cope with nitrosative stress and subvert host defenses. In bacteria, various transcription factors have been described which directly bind NO and serve as bona fide NO sensors to regulate adaptive responses to nitrosative stress (Spiro, 2007). Our laboratory previously showed that the NsrR transcription regulator of the enteric pathogen *Salmonella enterica* serovar Typhimurium induces a nitrosative stress resistance regulon that includes flavohemoglobin, an NO-detoxifying enzyme that is required for virulence (Bang et al., 2006; Karlinsey et al., 2012). Opportunistic pathogens like the Gram-positive bacterium *Staphylococcus aureus* lack NsrR to directly detect NO and instead rely on the two-component SrrAB system to detect impaired respiration and trigger upregulation of NO resistance genes (Kinkel et al., 2013; Richardson et al., 2006). In addition to flavohemoglobin, *S. aureus* encodes an NO-inducible lactate dehydrogenase that facilitates metabolic adaptation and replication in the presence of NO (Richardson et al., 2008; Vitko et al., 2015). Despite the relative resistance of *S. aureus* to NO-mediated growth inhibition, iNOS remains important for the control of staphylococcal infections (Li et al., 2014; McInnes et al., 1998; Richardson et al., 2008; Rothfork et al., 2004; Sasaki et al., 1998). Although numerous studies have established the impact of nitrosative stress on basic bacterial physiology, little is known about the effect of NO on the expression of virulence factors that influence the course of bacterial infections.

To better understand nitrosative stress responses in bacteria and the role of NO in staphylococcal virulence, we employed an unbiased biochemical approach to identify bacterial proteins that are susceptible to NO modification. Proteomic tools have recently been developed to identify eukaryotic proteins containing cysteine residues that are susceptible to *S*-nitrosylation, the reversible covalent modification of sulfhydryl groups (Doulias et al., 2010). To identify *S*-nitrosylated proteins in *S. aureus*, a clinically important human pathogen, we adapted mercury resin-assisted capture (MRC) followed by liquid chromatography-tandem mass spectrometry (LC-MS/MS). Here we show that the staphylococcal Agr quorum sensing (QS) system is susceptible to *S*-nitrosylation, identify the AgrA transcription factor as a direct molecular target of NO, and assess the effect of QS inhibition on virulence factor production in bacterial cultures and in a murine pneumonia model. Our findings demonstrate a protective role for host NO as an anti-virulence mediator in staphylococcal infections.

RESULTS

Staphylococcal Metabolic Enzymes and Agr QS are Susceptible to *S*-nitrosylation

A comprehensive proteomic analysis identified 210 unique *S*-nitrosocysteine residues in 5.8% of the total proteins encoded in the *S. aureus* genome (Figure S1 and Table S1). The dataset included constituents of carbohydrate and lipid metabolism (20.9%) as well as cell wall (5.7%), nucleotide (9.5%), tRNA (12.3%), cofactor (8.1%) and amino acid (6.6%) biosynthetic pathways (Figure 1A). Proteins with roles in protein translation (9.5%), transcription (7.1%), DNA replication and DNA repair (5.7%) were also detected. A small

percentage of the dataset consisted of proteins of unknown function (5.2%), and less represented pathways included proteins involved in protein stability (3.8%), cell redox (2.8%), antibiotic resistance and virulence (1.9%), secondary metabolite biosynthesis (0.7%), and secretion (0.7%). The predominance of metabolic enzymes and proteins important for bacterial physiology is consistent with the general growth inhibitory effects of NO on bacteria (Fang, 1999; Richardson et al., 2006; Richardson et al., 2008; Richardson et al., 2011).

Although virulence factors and regulators comprised only a small proportion of this dataset, AgrA, a central component of staphylococcal QS and major activator of virulence genes was found to be *S*-nitrosylated at cysteine residues C6, C123, and C199 within the response regulator (RR) receiver and DNA-binding domains (Figure 1C and Table S1). Modification of other AgrA cysteine residues was not detected (C55, C228). To further confirm AgrA as an NO target, the biotin-switch method in which NO-modified thiols are replaced with a stable biotin label was employed (Jaffrey and Snyder, 2001) (Figure S1B). In agreement with the proteomic analysis, biotin-switch showed *S*-nitrosylation of AgrA in lysates treated with NO, but not in untreated samples or in samples where *S*-nitrosylation was reversed with UV light prior to biotinylation (Figure 1B). Together these results show that AgrA cysteines are susceptible to chemical modification by NO.

NO Inhibits Transcription of the Agr Operon and Genes Regulated by QS

An earlier gene expression study from our laboratory had suggested possible NO inhibition of QS when the *hld* gene coding for δ-toxin was found to be downregulated in *S. aureus* cultures treated with NO (Richardson et al., 2006). The δ-toxin transcript is part of RNAIII, a small regulatory RNA and a hallmark of *S. aureus* QS (Novick and Geisinger, 2008). In staphylococci, QS is mediated by a multicomponent system encoded by the *agr* operon (Figure 2A). The QS signal, known as the auto-inducing peptide (AIP), is formed when the AgrD propeptide is cleaved and exported by the membrane-bound AgrB endopeptidase. As bacterial cell density increases, AIP accumulates extracellularly and binds the AgrC receptor. Upon binding, AgrC is auto-phosphorylated and activates the AgrA response regulator. AgrA phosphorylation results in positive auto-regulation via the *agrPII* promoter and the induction of additional promoters that trigger toxin production. Activation of *agrPIII* induces RNAIII, which post-transcriptionally stimulates expression of the cytolytic α-toxin and blocks translation of the Rot repressor of toxins (Boisset et al., 2007; Morfeldt et al., 1995). In addition, AgrA directly drives the expression of other virulence factors such as the phenol soluble modulins (PSMs) (Queck et al., 2008). To determine if *S*-nitrosylation disrupts the ability of AgrA to activate transcription, transcript levels from four independent Agr-regulated promoters were measured by RT-qPCR, and all transcripts (*agrA*, *agrB*, RNAIII, *psma* and *psmβ*) showed dose-dependent inhibition with increasing NO concentrations (Figure 2B). Transcription of the *proC* and *rpoD* housekeeping genes was unaffected, and the control NO-responsive flavohemoglobin (*hmp*) and *nrdG* genes were induced as expected (Figure 2B). Inhibition of the Agr system by NO was also evident in the clinically relevant *S. aureus* SF8300 (USA300) strain and occurred independent of transcription factors SarA and SarU, which were previously shown to modulate QS (Figure 2C–D). These experiments show that inhibition of QS results in the specific downregulation

of virulence genes controlled by AgrA and that the decrease in transcript levels is not the result of a global impairment of transcription.

S-nitrosylation of AgrA Mediates Inhibition of QS by NO

The susceptibility of cysteine residues to *S*-nitrosylation and the stability of this modification are dependent on their biochemical context within a protein (*e.g.* solvent accessibility, hydrophobicity and electrostatics). It is expected that some unstable modifications might not be detected by our proteomic approach. It is also important to note that not all cysteine modifications will necessarily affect protein function and mediate a biological effect. To determine the AgrA cysteine residues required for NO to inhibit QS, we performed site-specific mutagenesis to replace individual cysteines with NO-insensitive amino acids. When expressed ectopically, all AgrA cysteine mutants with the exception of C228 maintained functionality with similar activity to the wild-type allele. In the proteomic study, C6, C123, and C199 were each shown to be *S*-nitrosylated. However, site-specific mutagenesis showed that only a C199S mutation conferred a dramatic reduction in NO sensitivity (Figure 3D). C55S and C123N mutants displayed a modest reduction in NO-sensitivity, and a C6V mutant was as sensitive to NO as wild-type AgrA (Figure 3A–C).

As multiple AgrA cysteines are *S*-nitrosylated, and site-specific mutations exhibited varying effects on QS inhibition, it is possible that *S*-nitrosylation of multiple cysteines results in distinctive effects on AgrA protein function. Nevertheless, the C199S mutant showed the greatest resistance to NO. Given the location of C199 within the DNA-binding domain, disruption of DNA-binding is likely the primary mechanism by which NO disrupts AgrA protein function. AgrA belongs to the LytTR family of regulators which are widely distributed among bacteria as regulators of virulence and other diverse microbial processes. Intriguingly, many LytTR regulators show conservation of the NO-reactive cysteines identified in our study (Figure S2), suggesting that NO might impact such processes in other bacterial species.

In addition to AgrA, other Agr components with cysteine residues potentially susceptible to *S*-nitrosylation include AgrB, AgrC, and AgrD. An AIP biosynthesis mutant (*S. aureus ΔagrBD*) stimulated with spent medium from wild-type cultures retained NO-sensitivity, indicating that Agr is inhibited independent of AIP production (Figure 3E). Similarly, a mutant strain lacking AgrC cysteines (*S. aureus agrC* C91S C371S) also remained sensitive to NO (Figure 3F). Together these results show that NO inhibits the expression of QS-regulated genes by *S*-nitrosylation of AgrA (Figure 2A).

S-nitrosylation Disrupts AgrA Occupancy of Target Promoters

To gain further insight into the mechanism of QS inhibition, the effects of NO on AgrA protein stability and function were determined. As AgrA is auto-regulated, it was unsurprising that NO lowered *agrA* transcript (Figure 2B and Figure S3) as well as protein levels (Figure 4A). Protein stability assays showed no impact on AgrA abundance if NO treatment occurred after protein translation was inhibited with tetracycline (James et al., 2013) (Figure 4B), thereby excluding the possibility that NO enhances the rate of AgrA degradation. Instead, low transcript and protein levels result from impaired auto-activation of

the *agrPII* promoter. We reasoned that if native AgrA auto-regulation were eliminated by promoter replacement, AgrA transcript levels would become NO-insensitive while AgrA-activated genes would remain inhibited. This was confirmed using a strain carrying *agrA* on a plasmid driven by the T5X promoter, which exhibited low levels of RNAIII, *psma* and *psmβ* transcripts despite preserved *agrA* transcript levels (Figure S3). It was further predicted that increasing bacterial levels of activated AgrA would also protect against NO inhibition. Accordingly, AgrA activation with AIP-containing spent medium rescued inhibition of RNAIII (Figure 4C), but induction of AgrA was unable to restore RNAIII expression in the absence of spent medium.

Modification of AgrA cysteines, in particular C199 within the DNA-binding domain, is predicted to impair binding to AgrA-regulated promoters (Sun et al., 2012). To test whether NO decreases AgrA occupancy of the *agrPII* and *agrPIII* promoters, chromatin immunoprecipitation-qPCR (ChIP-qPCR) was performed. DNA proximal to AgrA binding sites, within the *agr* intergenic and RNAIII coding regions, showed specific ChIP-enrichment compared to control DNA regions (*gyrB*, *gmk*, *rpoD,* and $ChIP_C$) (Figure 4D). Importantly, AgrA promoter occupancy significantly decreased following NO treatment and was partially dependent on AgrA cysteines C55 and C199 (Figure 4D). ChIP-qPCR was not performed with *agrA* C55S C123N C199S, as this triple mutant protein is non-functional. Decreased promoter occupancy was not the result of inhibited auto-regulation, as AgrA was expressed from the T5X promoter in these experiments. We conclude that NO inhibits staphylococcal QS by impairing AgrA-mediated transcriptional activation of target promoters.

Host Production of NO is Protective against Staphylococcal Virulence in a Murine Pneumonia Model

S. aureus virulence is largely dependent on Agr QS. Mutants defective in Agr function are attenuated in multiple models of infection including endocarditis, pneumonia, osteomyelitis, septic arthritis and skin abscess (Novick and Geisinger, 2008; Thoendel et al., 2011). In the murine model of staphylococcal pneumonia, α-toxin mediates lung damage, increased inflammation and mortality (Bartlett et al., 2008; Bubeck Wardenburg et al., 2007a; Bubeck Wardenburg et al., 2007b). Mutant strains lacking Agr, α-toxin, or PSMs display reduced cytotoxicity toward human and murine immune cells (Kitur et al., 2015). Additionally, PSMα4-stimulated release of heparin-binding protein by neutrophils increases lung vascular leakage and contributes to pathogenesis (li et al., 2016).

To determine whether host-derived NO has a protective role *in vivo*, C57BL/6 mice and congenic iNOS knockout mice were challenged with wild-type *S. aureus* via an intranasal route. Mice were euthanized as they became moribund and displayed signs of increased disease severity including reduced mobility, hunched posture, and labored breathing. Strikingly, higher mortality was observed in iNOS knockout mice (8 of 15) compared to C57BL/6 (1 of 15 mice) (Figure 5A). As moribund mice succumb to infection, they experience a fall in body surface temperature, a sign associated with impending mortality (Bast et al., 2004). We monitored body surface temperature over 24 h post-infection and detected statistically significant differences between C57BL/6 and iNOS knockout mice

from 8–12 h post-infection (Figure S4). Body surface temperature was notable for multiple measurements below 25°C in mice that became moribund, whereas surviving mice approached 25°C before rebounding (Figure S4). Continuous monitoring of mouse body surface temperature thus provided an objective approach to assess disease severity and showed that iNOS knockout mice develop more severe staphylococcal pneumonia compared to C57BL/6 mice.

As NO can slow staphylococcal growth (Richardson et al., 2008), we determined the bacterial burden of mice at 8 h post-infection. Despite finding statistically significant differences in body surface temperature between C57BL/6 and congenic iNOS-deficient mice, there were no significant differences in lung bacterial burden (Figure 5B) suggesting that the protective effect of NO in staphylococcal pneumonia cannot be attributed to the bacteriostatic properties of NO. Rather, the protective effects of NO in C57BL/6 mice may result from the inhibition of Agr QS and reduced production of virulence factors, as observed *in vitro*. As the Agr-regulated α-toxin plays a critical role in lung damage and inflammation, serum cytokine levels in wild-type and iNOS-deficient mice were compared. Serum levels of multiple pro-inflammatory cytokines including KC, MCP-1, IL-17A, and TNFα were significantly higher in the iNOS knockout mice than in congenic C57BL/6 controls (Figure 5B). A higher trend for IL-6 ($p = 0.06$) was also observed (Figure 5B). In previous studies, KC and Th17 cytokine responses were found to be stimulated by α-toxin and were associated with poor outcomes in staphylococcal pneumonia (Bartlett et al., 2008; Frank et al., 2012; Martin et al., 2011). Similarly, higher levels of IL-6, MCP-1, and TNFα have correlated with worsened clinical outcomes (Kitur et al., 2015; Parker et al., 2015; Robertson et al., 2008; van den Berg et al., 2013).

The administration of increased bacterial inocula abrogated NO-dependent differences in disease severity (as indicated by body surface temperature) (Figure 5B) and pro-inflammatory cytokine responses (Figure 5B), indicating that the protective actions of NO can be overwhelmed by high bacterial burdens. Nevertheless, the analysis of individual mice showed that disease severity correlates with bacterial burden only in wild-type but not in iNOS-deficient mice, after both low and high bacterial inocula (Figure S5), whereas linear regression analysis revealed a negative relationship between disease severity and serum levels of pro-inflammatory cytokines IL-6, IL-17A, and KC in all mice, consistent with the role of differential α-toxin production in the protective actions of NO during staphylococcal pneumonia. Collectively, these results suggest that NO protects the host by inhibiting the expression of bacterial virulence factors that promote inflammatory responses.

Increased virulence factor production in iNOS-deficient mice during staphylococcal pneumonia is expected to result in different lung inflammatory responses. At 4 h post-infection, histologic changes between C57BL/6 and iNOS knockout mice were subtle. However, by 8 h post-infection morphological patterns distinguishing C57BL/6 and iNOS-deficient mice became evident (Table S2). Lungs from C57BL/6 mice displayed numerous highly cellular, focal-to-confluent aggregations of densely packed neutrophils with few mononuclear cells (Figure 6 and Figure S6). These foci, scattered throughout the lung section, surround blood vessels and small bronchioles, variably involving adjacent alveolar walls (Figure 6B). Clusters of bacteria and necrotic debris were evident particularly within

the centers of aggregates (Figure 6B). At 8 h post-infection, these inflammatory cell aggregates were morphologically consistent with early-stage abscess formation. In contrast, lungs from iNOS-deficient mice exhibited more diffuse infiltration of inflammatory cells with many bacteria and an interstitial distribution that was predominately localized along alveolar walls (Figure 6, Figure S6, and Table S2). Some gender-dependent differences were noted, with less distinct and less prominent inflammatory cell accumulations in females than was observed in males (Table S2). At the lower inoculum, female mice showed a further reduction in inflammation, although the basic trends remained (Figure S6). The distinctive histopathological differences observed between C57BL/6 and congenic iNOS knockout mice are consistent with a different immune response and ability to control infection resulting from differences in virulence factor production, further highlighting the protective role of host NO in staphylococcal pneumonia.

Alpha-toxin is a major contributor to pathogenesis in staphylococcal pneumonia, and differences in disease severity between C57BL/6 and iNOS knockout mice may be explained by different levels of α-toxin production. Furthermore, our *in vitro* findings showing that NO inhibits QS by targeting AgrA suggested the possibility that iNOS protects the host by limiting toxin production *in vivo*. To determine whether *S. aureus* produces higher levels of α-toxin in iNOS-deficient mice compared to C57BL/6 mice, total levels of α-toxin per lung were measured by ELISA from lung homogenates (Berube et al., 2014). Although there were no significant differences in bacterial burden at 8 h post-infection, significantly higher levels of α-toxin were produced in iNOS-deficient mice compared to C57BL/6 mice (Figure 7). Importantly, differences in α-toxin levels were abrogated when mice were infected with an *S. aureus* site-specific cysteine double mutant (*agrA* C55S C199S) that is insensitive to NO inhibition (Figure S7A). Infections with a triple cysteine mutant (*agrA* C55S C123N C199S) could not be performed, as the triple mutant protein was non-functional. Despite increased production of α-toxin in C57BL/6 mice infected with *agrA* C55S C199S compared to wild-type *S. aureus*, we did not find a difference in mortality that would indicate hypervirulence of the NO-insensitive mutant (Figure S7B). Nevertheless, the role of NO in limiting α-toxin production during staphylococcal pneumonia and its dependence on AgrA cysteine residues provides strong evidence that NO modulates staphylococcal virulence *in vivo*.

DISCUSSION

NO is a versatile molecule that plays a central role in host innate immunity. Organisms ranging from bacteria to plants and mammals have evolved diverse mechanisms to produce and sense NO at low non-cytotoxic levels where it serves as an important signaling molecule (Crane et al., 2010; Domingos et al., 2015; Förstermann and Sessa, 2012; Plate and Marletta, 2013). In mammalian hosts, the generation of high cytotoxic NO concentrations by innate immune cells provides an effective antimicrobial mechanism that limits pathogen growth during infection. NO production is essential for host resistance to the human pathogen *Staphylococcus aureus* even though *S. aureus* is resistant to growth inhibition by NO *in vitro* (Richardson et al., 2008). This study was undertaken to better understand the mechanism of NO-mediated protection during staphylococcal infections.

A proteomic analysis identified a large number of staphylococcal proteins susceptible to *S*-nitrosylation, many of which are conserved in other bacteria. The large number of targets is consistent with the known pleiotropic properties of NO and its diverse effects on bacterial physiology. As NO is able to inhibit growth of many organisms, it was not surprising to find that NO is able to modify many metabolic enzymes and other proteins responsible for basic physiological processes. However, we were interested to discover that NO modifies AgrA, the response-regulator of the Agr QS system, which plays a central role in staphylococcal pathogenesis. This anti-virulence mechanism is consistent with previous studies that show host factors such as apolipoprotein B and Nox2 can sequester and modify the staphylococcal AIP signaling peptide to inactivate QS (Peterson et al., 2008; Hall et al., 2013; Manifold-Wheeler et al., 2016; Rothfork et al., 2004).

We subsequently demonstrated that *S*-nitrosylation of AgrA impairs the transcription of QS-regulated virulence factors. The inhibitory effect of NO on the Agr QS system is largely dependent on a single cysteine target (C199) in AgrA. The Agr system has multi-components with several critical cysteine residues that are required for function. The AgrD pro-peptide, which is processed into the AIP signal molecule, forms a thiolactone ring through its sole cysteine residue, and the AgrB endopeptidase requires a catalytic cysteine to cleave AgrD during peptide processing (Qiu et al., 2005; Thoendel and Horswill, 2009; Thoendel and Horswill, 2012). The cysteines in the AgrC sensor kinase have not been implicated in Agr function but in principle might have mediated NO inhibition by preventing signal transduction upon AIP binding. However, no Agr component other than AgrA was detected in our proteomic study, and *agrBD* null and AgrC site-specific mutants lacking cysteine remain sensitive to NO. Although highly oxidative species such as hypochlorite and peroxynitrite have been shown to inactivate QS by oxidizing the methionine residue of AIP (Rothfork et al., 2004), NO reactivity in the absence of other oxidants (*e.g.* superoxide) is limited to metal centers, thiols, and other radicals. Multiple cysteine thiols in AgrA are subject to *S*-nitrosylation, and the AgrA C199S mutation confers resistance to NO *in vitro*. The mechanism of QS inhibition highlights the importance of molecular context for protein cysteines to undergo *S*-nitrosylation and elicit a physiological response. The sensitivity of AgrA C199 to NO demonstrated in our study, along with the susceptibility of this residue to oxidation by H_2O_2 (Sun et al., 2012), suggests that this residue has evolved to integrate redox signaling with QS. Interestingly, we found that an *S. aureus* mutant (*agrA* C55S C199S) that is highly insensitive to NO was not hypervirulent in C57BL/6 mice despite producing higher levels of α-toxin than wild-type *S. aureus.* This may be explained by a dual role of AgrA C199 in sensing both NO and H_2O_2. Sun et al demonstrated that mutations at C199 sensitize *S. aureus* to H_2O_2 *in vitro*, suggesting that a C199 mutation would result in virulence attenuation *in vivo.*

The protective actions of NO during staphylococcal infection despite the ability of *S. aureus* to grow in the presence of high NO levels that are cytotoxic for other bacteria are most likely attributable to the repression of staphylococcal virulence gene expression by NO. Consistent with this hypothesis, iNOS-deficient mice showed no significant difference in bacterial burden at 8 h post-infection despite a dramatic difference in disease severity as indicated by increased mortality, hypothermia, higher inflammatory cytokine responses, and distinctive lung histopathology. The inhibition of *S. aureus* virulence gene expression by NO *in vitro*

and lower α-toxin levels in iNOS-competent mice, along with the decreased cytokine/chemokine responses known to be dependent on the Agr-regulated α-toxin, further support a role of NO in repressing bacterial virulence. Alveolar and interstitial macrophages are appropriately situated to detect lung pathogens and regulate inflammatory responses (Hussell and Bell, 2014; Kopf et al., 2015). In the murine pneumonia model, lung macrophages represent a possible source of NO, although a contribution from airway epithelial cells cannot be excluded.

A protective role for NO in bacterial pneumonia has also been demonstrated for *Streptococcus pneumoniae* and other lung pathogens (Yang et al., 2014). Interestingly, Yang et al. showed the role for eNOS (endothelial NO synthase, NOS3) in pneumococcal pneumonia to be gender-specific. Overall, we did not find the protective role of iNOS in staphylococcal pneumonia to be gender-dependent, although some histological differences were observed. Our findings contrast somewhat with an earlier study that failed to observe an effect of iNOS on mouse survival in staphylococcal pneumonia (Köhler et al., 2011). However, we note differences in the inoculum size and bacterial culture conditions between the two studies and found that a modest difference in inoculum had a substantial impact on clinical outcomes. Collectively, the earlier study by Köhler et al and the present study indicate that the protective role of iNOS is abrogated by infection with inocula $>1 \times 10^8$ CFU but is evident after the administration of 5×10^7 CFU, as indicated by mouse mortality, body surface temperature, and serum cytokine levels (Figure 5).

A previous study of staphylococcal pneumonia showed that mice infected with *S. aureus* strains producing α-toxin have higher levels of the KC chemokine and more neutrophil influx into the airways than mutants lacking α-toxin (Bartlett et al., 2008). Consistently, we found that iNOS-deficient mice, which show higher levels of α-toxin in the lung than C57BL/6, also have higher serum levels of the KC neutrophil chemoattractant. Our histopathological observations identify a different pattern of lung lesions in C57BL/6 mice compared to iNOS-deficient mice. C57BL/6 mice show focal aggregates of inflammatory cells, whereas iNOS-deficient mice show a diffuse pattern. This qualitative difference in the lung distribution of inflammatory cells (focal vs diffuse) limits any specific quantitative interpretation with regard to neutrophil recruitment, as the general composition of the inflammatory cell population has not been determined. Another important distinction between our study and that of Bartlett et al is that NO-expressing C57BL/6 mice only reduce the levels of α-toxin produced during infection, whereas infections with α-toxin mutants would likely result in more dramatic effects on the inflammatory response.

As a commensal and opportunistic human pathogen, *S. aureus* is highly adapted to the selective pressures imposed on bacteria by host immunity. Inhibition of QS by NO may have evolved to maintain a stable relationship between *S. aureus* and the human host. Other scenarios have been described in which staphylococcal immune evasion factors appear to have evolved to directly interact with immune molecules (Thammavongsa et al., 2015). The ability to coordinate virulence factor production in response to host immune responses may provide an evolutionary advantage for *S. aureus* when it encounters the high NO concentrations present in the human nose (Lundberg et al., 1995), where downregulation of exotoxins might help to maintain the bacteria in a commensal state. Indeed, humans with

persistent asymptomatic *S. aureus* nasal carriage have been shown to exhibit low expression levels of Agr-activated genes (Burian et al., 2010), although the molecular basis for this observation remains to be determined. A dual role as commensal and pathogen might explain why staphylococci maintain a QS system that is sensitive to NO.

It is increasingly appreciated that inter-bacterial communication in both commensal and pathogenic bacteria is important to coordinate group behavior in complex bacterial communities. Our observations show that a ubiquitous host-derived mediator can ameliorate the consequences of infection by interfering with cell-to-cell communication in *S. aureus.* Regulators similar to AgrA, belonging to the LytTR family, control diverse bacterial processes and are widely distributed in other clinically important pathogens (*e.g. Clostridium, Enterococcus, Listeria, Streptococcus, Klebsiella*) (Galperin, 2008). Modulation of QS, virulence, and other bacterial processes by NO may prove to be a widespread phenomenon.

STAR METHODS

CONTACT FOR REAGENT AND RESOURCE SHARING

Further information and requests for resources and reagents should be directed to and will be fulfilled by the Lead Contact, Ferric C. Fang (fcfang@uw.edu).

EXPERIMENTAL MODEL AND SUBJECT DETAILS

Bacterial strains and growth conditions—Bacterial strains used in this study are listed in the Key Resources Table. *S. aureus* HG003 (Herbert et al., 2010) was used for *in vitro* experiments and *S. aureus* Newman for animal studies. Unless otherwise indicated, *S. aureus* cultures were grown in tryptic soy broth (TSB) at 37°C with shaking at 250 rpm. For plasmid retention, 10 μg ml^{-1} chloramphenicol was used when appropriate. To induce AgrA expression from the T5X promoter, TSB was supplemented with 2% xylose. *E. coli* strains for plasmid construction were grown in Luria-Bertani broth (LB) with 100 μg ml^{-1} ampicillin.

Spent medium used in experiments to stimulate Agr activity was prepared from *S. aureus* HG003 cultures of an optical density (OD_{600nm}) of 5.0. Bacteria were pelleted by centrifugation and supernatants filter-sterilized with a 0.2 μm polyethersulfone syringe filter (ThermoFisher Scientific).

Experimental animals—Animal experiments were approved by the University of Washington Institutional Animal Care and Use Committee (Protocol #3373-01). Investigators were not blinded, and animal studies were non-randomized. No statistical method was used to predetermine sample size. C57BL/6 and congenic iNOS knockout mice were purchased from Jackson Laboratories (Bar Harbor, ME), then bred and maintained under specific pathogen-free conditions at the University of Washington Animal Care and Research Facility. Mice were maintained on a 14-hour light cycle and housed up to 5 animals per cage; mice under ABSL-2 containment were housed in Allentown cages with micro-isolator tops. Mice were checked hourly during infection studies. Veterinary care was

provided 7 days a week. Animal studies were gender-matched, and mice were 11–15 weeks old.

METHODS DETAILS

Construction of plasmids—Plasmids and primers used in this study are listed in the Key Resources Table and Table S3, respectively. Inducible AgrA expression systems with untagged and HA-tagged C-termini were constructed by PCR-amplification and restriction enzyme-based cloning. PCR amplicons of *agrA* with its native ribosomal binding site were digested with BamHI and KpnI (Fermentas) and ligated into pEPSA5 (Forsyth et al., 2002). Primer pairs RU106-RU107 and RU106-RU116 were used to construct p*agrA* and p*agrA-HA*, respectively. Mutant plasmid derivatives of p*agrA* were generated using the QuikChange Lightning Site-Directed Mutagenesis Kit (Agilent Technologies) with primer pairs indicated in Table S3.

Allelic exchange mutagenesis plasmids were constructed by SOE-PCR as previously described (Monk et al., 2012). For pIMAYΔ*agrA,* ~1 kbp regions were PCR-amplified upstream of the *agrA* start site and downstream of the stop site with RU044-RU045B and RU048B-RU049, respectively. To join the amplicons, SOE-PCR was carried out with RU044A-RU049AA yielding an *agrA* deletion cassette. The deletion cassette was cloned into pIMAY at the KpnI and NotI restriction sites. pIMAYΔ*agrC* was constructed similarly with RU076-RU077 to amplify the upstream region and RU078-RU079 the downstream region. Primer pair RU076-RU079 was used for SOE-PCR. pIMAYΔ*sarA* was constructed with primers RU096-RU097 and RU098-RU099.

To generate pIMAY*agrA* C55S C199S, a PCR fragment amplified with RU044AA-RU049AA from genomic DNA was ligated into pIMAY at KpnI and NotI sites. Site-specific mutagenesis was performed twice using the QuikChange Lightning Site-Directed Mutagenesis Kit (Agilent Technologies) with primers RU070-RU071 and RU050-RU051.

To generate pIMAY*agrA-HA* for allelic replacement, a PCR fragment containing *agrA* plus its ~1 kbp upstream region was amplified with RU044-RU138. The downstream region was amplified with RU139-RU049. Primer pair RU044-RU049 was used for SOE-PCR.

To generate pIMAY*agrC* C91S C371S, a PCR amplicon was generated using primer pair RU076-RU079 and cloned into pIMAY at KpnI and NotI. The QuikChange Lightning Site-Directed Mutagenesis Kit (Agilent Technologies) was used to introduce site-specific mutations with primer pairs RU080-RU081 and RU082-RU083.

All plasmid constructs were initially electroporated into *E. coli* DH10B ElectroMAX (Invitrogen), isolated with the QIAprep Spin Miniprep Kit (QIAGEN) and electroporated into the restriction-deficient cloning host *S. aureus* RN4220 (Kreiswirth et al., 1983). Plasmids were then transduced via ϕ-11 into experimental strains as previously described (Novick, 1991).

Construction of mutants—Allelic exchange mutagenesis was performed as previously described (Monk et al., 2012). RU111 was generated from *S. aureus* HG003 with

pIMAYΔ*agrA* and was subsequently used to generate RU226 with pIMAY*agrA-HA*. RU141 was generated from *S. aureus* HG003 with pIMAYΔ*agrC* and subsequently used to generate RU161 with pIMAY*agrC* C91S C371S. Spontaneous mutant RU371 was selected for streptomycin resistance in tryptic soy agar plates containing 250 μg ml^{-1} streptomycin and used to generate RU373 with pIMAYΔ*agrC*. Strain RU498 was constructed from RU371 using pIMAYΔagrA and then RU516 was subsequently generated using pIMAY*agrA* C55S C199S.

Mercury resin assisted capture and mass spectrometry—Overnight *S. aureus* HG003 cultures were diluted $1:10^2$ in 250 ml TSB and grown to an OD_{600nm} of 2.0. Bacteria were pelleted and washed once with 50 ml PBS. Bacteria were resuspended in 6 ml lysis buffer (250 mM HEPES pH 7.7, 1 mM DTPA, 0.1 mM neocuproine, 1% Triton X-100), incubated with 100 μg ml^{-1} lysostaphin (AMBI Products) for 15 min at 37°C and then placed on ice. The cOmplete Protease Inhibitor Cocktail (Roche) was added and bacteria were French-pressed twice at 20,000 psi. Cell debris was removed by centrifugation at 10,000 rcf for 15 min at 4°C. To remove low molecular weight thiols, lysates were dialyzed twice overnight with a 3,500 MWCO Slide-A-Lyzer dialysis cassette (ThermoFisher Scientific) in 1 L of lysis buffer. Ten ml of 0.8 mg ml^{-1} protein were *S*-nitrosylated with 150 μM diethylamine NONOate (DEA/NO) (Cayman Chemical) for 10 min at 37°C. A control sample was treated in parallel with 150 μM diethylamine (DEA) (Sigma-Aldrich). NO treatment was stopped by precipitating protein in ice-cold 75% acetone and incubating for 20 min at −20°C. Samples were washed once with 75% acetone and resuspended in 10 ml blocking buffer (250 mM HEPES pH 7.7, 1 mM DTPA, 0.1 mM neocuproine, 2.5% SDS). Unmodified protein cysteines were chemically blocked with 50 mM N-ethylmaleimide (NEM) (Sigma-Aldrich) for 60 min at 50°C. Samples were vortexed every 5 min. NEM blocking was stopped by precipitating in ice-cold 75% acetone and incubating for 20 min at −20°C. Samples were washed four times with 75% acetone and resuspended in 4 ml loading buffer (250 mM MES pH 6.0, 1 mM DTPA, 1% SDS).

Mercury resin assisted capture was performed as previously described (Doulias et al., 2010). Foil-wrapped Econo-Pac chromatography columns (Bio-Rad Laboratories, inc) were filled with a 4 ml bed of mercury resin and 40 ml of isopropanol passed through the column, followed by 80 ml deionized H_2O, and 80 ml of 0.1 M $NaHCO_3$ (pH 8.8). To equilibrate, 80 ml equilibration buffer (50 mM MES pH 6.0, 50 mM NaCl, 1 mM DTPA) was passed through the column. Samples were added by gravity flow and incubated for 1 h. Columns were washed with 200 ml wash buffer (50 mM Tris-HCl pH 7.5, 0.3 M NaCl) containing 0.5% SDS, 200 ml wash buffer containing 0.05% SDS, 200 ml wash buffer containing 1% Triton X-100 plus 1 M urea, 200 ml wash buffer containing 1% Triton X-100 plus 0.1 M urea, and then washed with 800 ml deionized H_2O. Trypsin digest was performed overnight for ~16 h with 5 mL of 1 μg mL^{-1} Trypsin Gold (Promega Corporation) in 0.1 M NH_4HCO_3. Columns were then washed with 160 ml of 1 M NH_4HCO_3 containing 0.3 M NaCl, 160 ml of 1 M NH_4HCO_3, 160 ml of 0.1 M NH_4HCO_3, and 800 ml deionized H_2O. To elute peptides, 6 ml performic acid were added and columns were incubated for 45 min before 6 ml of deionized H_2O were added. Eluted samples were lyophilized and sent for LC-MS/MS analysis at the Protein Core in Children's Hospital of Philadelphia Research

Institute (Philadelphia, PA). Tryptic peptide digests were analyzed by hybrid-Orbitrap Elite mass spectrometer (Thermo Electron, San Jose, CA). A schematic of this protocol is shown in Figure S1A.

Generation and evaluation of SEQUEST peptide assignments—The post mass spectrometry analysis has been previously described in detail (Doulias et al., 2010). In brief, the raw files, which contain the MS/MS spectra were submitted to Sorcerer Sequest (Sage-N Research, Inc) for database search and generation of potential sequence-to-spectrum peptide assignments. A *S. aureus* database comprising 10,982 entries (canonical and isoform sequences) was used. Database search included cysteine trioxidation (+48Da), methionine dioxidation (+32Da) and alkylation of cysteine by N-ethylmaleimide (+125Da) as differential modifications. Scaffold Version 4. 0. 4 (Proteome Software) was used to validate protein identifications and perform manual inspection of MS/MS spectra. Empirically defined X_{corr} thresholds were applied to filter cysteic-acid and non-modified peptides independently so the false discovery rate (FDR) was ≤ 1%. Finally, all cysteine-containing spectra were manually inspected based on previously defined criteria (Doulias et al., 2010).

Biotin-switch of HA-tagged AgrA—The biotin-switch method was adapted and modified from a previous study (Jaffrey and Snyder, 2001). Overnight RU198 cultures were diluted $1:10^2$ in 100 ml TSB and grown to an OD_{600nm} of 0.6. Cultures were induced with 2% xylose until cultures reached an OD_{600nm} of 5.0. Bacteria were pelleted and washed once with 50 ml PBS. Bacteria were resuspended in 8 ml lysis buffer (250 mM HEPES pH 7.7, 1 mM DTPA, 0.1 mM neocuproine, 1% Triton X-100) and incubated with 100 μg ml^{-1} lysostaphin (AMBI Products) for 30 min at 37°C. The cOmplete Protease Inhibitor Cocktail (Roche) was added and bacteria were sonicated with a Microson Ultrasonic Cell Disruptor XL (Misonix). Cell debris was removed by centrifugation at 10,000 rcf for 15 min at 4°C. Low molecular weight thiols were removed with Econo-Pac 10DG desalting columns (BD Biosciences) following manufacturer's recommendations. Total protein concentration was determined using the Coomassie Protein Assay Kit (ThermoFisher Scientific). Two 3 ml samples (1 mg ml^{-1}) were treated in dark conical tubes with 1 mM DEA/NO (Cayman Chemical) for 10 min at 37°C. A control sample was treated in parallel with 1 mM DEA (Sigma-Aldrich). To stop *S*-nitrosylation, samples were precipitated in ice-cold 75% acetone and incubated for 20 min at −20°C. Samples were washed once with 75% acetone and resuspended in 3 ml blocking buffer (250 mM HEPES pH 7.7, 1 mM DTPA, 0.1 mM neocuproine, 2.5% SDS). As an additional negative control, one of the two DEA/NO-treated samples was exposed to ultraviolet light for 25 min to denitrosylate proteins. Samples were blocked with 40 mM MMTS for 90 min at 50°C with vortexing every 5 min. MMTS blocking was stopped by precipitating in ice-cold 75% acetone and incubating for 20 min at −20°C. Samples were washed 4 times with 75% acetone and resuspended in 1 ml labeling buffer (250 mM HEPES pH 7.7, 1 mM DTPA, 0.1 mM neocuproine, 1% SDS). To label *S*-nitrosylated proteins, samples were incubated for 90 min with 20 mM sodium L-ascorbate (Sigma-Aldrich) and 400 μM EZ-Link HPDP-Biotin (ThermoFisher Scientific). To stop biotinylation, samples were precipitated in ice-cold 75% acetone and incubated for 20 min at 20°C. Samples were washed once in 75% acetone and resuspended in 1 ml resuspension buffer (250 mM HEPES pH 7.7, 1 mM DTPA, 0.1 mM neocuproine, 0.1% SDS). Protein

concentration was determined and 75 μg of biotin-labeled protein immunoprecipitated with Pierce Anti-HA Magnetic Beads (ThermoFisher Scientific) following manufacturer's recommendations. AgrA-HA was eluted using SDS-PAGE sample buffer, subjected to SDS-PAGE and transferred onto a low-fluorescence PVDF transfer membrane (ThermoFisher Scientific). Western blots were probed with Alexa 488 anti-hemagglutinin mouse monoclonal 16B12 antibody (Molecular Probes) and Alexa 647 streptavidin conjugate (Molecular Probes). A FluorChem Q imaging system (Alpha Innotech) was used to visualize western blots and ImageJ Version 1.47 Software (Wayne Rasband, U. S. National Institutes of Health) used for densitometry. A schematic of this protocol is shown in Figure S1B.

Reverse transcription quantitative real-time PCR—Overnight *S. aureus* HG003 cultures were diluted $1:10^2$ in 30 ml TSB and grown to an OD_{600nm} of 0.6. Cultures were treated with propylamine propylamine NONOate (PAPA/NO) (Cayman Chemical) for 45 min in 3 ml volumes. After NO treatment, 0.4 ml samples were immediately placed in RNAprotect Bacterial Reagent (QIAGEN) and incubated for 5 min at room temperature. Bacteria were pelleted and saved overnight at −20°C. Cells were lysed with 100 μg ml^{-1} lysostaphin (AMBI Products) by incubating for 30 min at 37°C. RNA was extracted using the RNeasy Mini Kit (QIAGEN) and treated with RNase-Free DNase (QIAGEN) according to the manufacturers recommendations. cDNA was synthesized using 500 ng RNA with the QuantiTect Reverse Transcription Kit (QIAGEN). The Quantifast SYBR Green PCR Kit (QIAGEN) and a CFX96 Real Time System (Bio-Rad) were used to perform qPCR. Data were analyzed using the comparative C_T method ($2^{-\Delta\Delta C_T}$) (Schmittgen and Livak, 2008) with the housekeeping gene *gyrB* as an internal control and normalized to an untreated sample. Primers used for qPCR are listed in Table S3. Primers for housekeeping genes and nitric oxide induced genes were based on previous studies (Goerke et al., 2000; Hirschhausen et al., 2012; Richardson et al., 2006; Theis et al., 2007).

Western blots and protein stability assays—Overnight RU083 and RU226 cultures were diluted $1:10^2$ in 26 ml TSB and grown to an OD_{600nm} of 0.6. Cultures were treated with 8 mM PAPA/NO (Cayman Chemical) for 45 min. Fifteen min after adding PAPA/NO, cultures were stimulated with 20% spent medium. Bacteria were pelleted and washed once with 30 ml PBS. Bacteria were resuspended in 1 ml lysis buffer (Tris HCl pH 7.5, 100 mM NaCl) and incubated with 100 μg ml^{-1} lysostaphin (AMBI Products) for 30 min at 37°C. Cell debris was removed by centrifugation at 18,000 rcf and protein concentration was determined using the Coomassie Protein Assay Kit (ThermoFisher Scientific). To improve the western blot signal, 1 mg total protein was immunoprecipitated with Pierce Anti-HA Magnetic Beads (ThermoFisher Scientific) as recommended by the manufacturer. Protein binding to beads was done overnight at 4°C. AgrA-HA was eluted with SDS-PAGE sample buffer by incubating at 95°C for 10 min. Immunoprecipitated samples were subjected to SDS-PAGE and transferred onto a low-fluorescence PVDF transfer membrane (ThermoFisher Scientific). SuperSignal Western Blot Enhancer (ThermoFisher Scientific) was used to improve the western blot signal. Western blots were probed with Alexa 488 anti-hemagglutinin mouse monoclonal 16B12 antibody (Molecular Probes). A FluorChem Q imaging system (Alpha Innotech) was used to visualize western blots and ImageJ Version 1.47 Software (Wayne Rasband, U. S. National Institutes of Health) used for densitometry.

Protein stability assays were performed similarly, except that total protein translation was inhibited with 10 μg ml^{-1} tetracycline 15 min prior to NO treatment. Samples were collected from cultures immediately before adding tetracycline and at 45 min and 90 min after adding PAPA/NO.

Chromatin immunoprecipitation-qPCR—Overnight RU198 cultures were diluted 1:10^2 in 80 ml TSB and grown to an OD_{600nm} of 0.6. The Agr system was stimulated with 20% spent medium and 2% xylose. Cultures were immediately treated with 6 mM PAPA/NO for 45 min. DNA was cross-linked with 1.5% formaldehyde (Macron Fine Chemicals) for 23 min at 30°C with shaking at 100 rpm. Cultures were quenched with 300 mM glycine (Sigma-Aldrich) for 5 min at 30°C with shaking at 100 rpm. Bacteria were pelleted and washed once with 40 ml PBS. Bacteria were resuspended in 1 ml lysis buffer (50 mM HEPES pH 7.5, 140 mM NaCl, 1 mM EDTA, 1% Triton X-100, 0.1% Na-deoxycholate), then incubated with 100 μg ml^{-1} lysostaphin (AMBI Products) for 30 min at 37°C. The cOmplete Protease Inhibitor Cocktail (Roche) was added and samples placed on ice for 10 min. FastProtein Blue Matrix (MP Biomedicals) was used to bead-beat samples three times for 30 sec at maximal speed with a Mini-Beadbeater (BioSpec Products). Cell debris was removed by centrifugation and DNA sheared by sonication with a Microson Ultrasonic Cell Disruptor XL (Misonix) for 8 rounds of fifteen 1 sec pulses.

Sheep anti-mouse IgG Dynabeads M-280 (Novex) were incubated in 750 μl blocking buffer (5 mg ml^{-1} BSA in PBS) for 30 min at 4°C. 1.5 μg of HA-7 mouse monoclonal anti-HA antibody (Sigma-Aldrich) was bound to beads for 3 h at 4°C in 750 μl blocking buffer. Beads were washed twice with 1 ml ice-cold washing buffer (100 mM Tris pH 8.0, 250 mM LiCl, 0.5% NP-40, 0.5% Na-deoxycholate, 1 mM EDTA), resuspended in 60 μl blocking buffer, and 12.5 ug of total protein were added. Volumes were adjusted to 750 μl with lysis buffer and samples incubated for 3 h at 4°C. Samples were washed twice for 5 min at 4°C with 600 μl lysis buffer, twice with 600 μl wash buffer, and once with 600 μl TE buffer pH 8.0 (Ambion). Samples were eluted in 120 μl TE buffer pH 8.0 (Ambion) with 1% SDS by incubating for 15 min at 65°C.

Cross-links were reversed by adding 130 μl TE buffer pH 8.0 (Ambion) with 1% SDS and incubating at 65°C for 15 h. Samples were diluted with 240 μl TE buffer pH 8.0, 20 μl of 10 mg ml^{-1} Proteinase K (Ambion) was added, and samples incubated at 45°C for 2 h. Fifty μl of 5 mM LiCl were added prior to extracting DNA with 400 μl UltraPure Phenol:Chloroform:Isoamyl Alcohol (Invitrogen). Two μl of 20 mg ml^{-1} glycogen (ThermoFisher Scientific) were added to extracted DNA and samples precipitated with 0.7 volumes of isopropanol at −80°C for 30 min. DNA was pelleted and washed once with 70% ethanol before DNA was air-dried and resuspended in 200 μl H_2O.

qPCR was performed with the Quantifast SYBR Green PCR Kit (QIAGEN) and a CFX96 Real Time System (Bio-Rad). Enrichment of DNA regions was calculated by the % input method relative to the *ChIPc* control DNA region located several kilobases away from the *agr* intergenic region (test DNA in ChIP sample/test DNA in input sample)/(*ChIPc* in ChIP sample/*ChIPc* in input sample) (Merrikh et al., 2015). Primers used for qPCR are listed in Table S3.

Bioinformatics—AgrA protein graphics were generated with PyMOL Molecular Graphics System Version 1.8 (Schrödinger, LLC). The structure of the DNA binding domain was downloaded from PDB (3BS1) and the response regulator (RR) receiver domain was modeled using Phyre2 (Kelley et al., 2015; Sidote et al., 2008). The AgrA amino acid sequence alignment was generated with Clustal Omega (Sievers et al., 2011) and the graphic rendered with MacVector Version 12.0.3 (MacVector, Inc).

Mouse infections and cytokine measurements—Mice were infected based on a previously developed murine pneumonia model (Bubeck Wardenburg et al., 2007b). Overnight RU371 and RU373 cultures were diluted 1:10^2 in 100 ml TSB and grown to an OD_{600nm} of 0.6. Bacteria were pelleted, washed once with 1 ml PBS and resuspended in 750 μl (cytokine study) or 1500 μl PBS (24 h surface temperature study). Mice were anesthetized with 3% isoflurane prior to delivering 30 μl of a bacterial inoculum (~1×10^8 or ~5×10^7 CFU, cytokine study; 5×10^7 CFU for 24 h surface temperature study) into the left nostril. Mice were held in the upright position for 1 min to allow aspiration. Body surface temperature was measured over the lower abdomen using a MiniTemp MT6 scanning infrared thermometer (Raytek). Moribund mice displaying low mobility, hunched posture, difficulty breathing, and had surface temperature below 25°C were euthanized using CO_2.

For the cytokine study, blood was collected by cardiac puncture immediately after CO_2 euthanasia. Blood was allowed to clot at room temperature and serum separated by centrifugation at 18,000 rcf for 5 min. Serum was collected and stored at −80°C until needed for cytokine measurements. Lungs were surgically removed, placed in 1 ml PBS on ice, and homogenized using a PowerGen 125 homogenizer (Fisher Scientific). To determine lung bacterial burden, homogenate dilutions were plated onto TSA plates with 250 μg ml^{-1} streptomycin.

To measure cytokines, serum was thawed on ice and cytokine levels determined with the Cytometric Bead Array Mouse Kit (BD Biosciences) and Mouse Enhanced Sensitivity Kit (BD Biosciences). Data was collected at the University of Washington Pathology Flow Cytometer Core Facility using an LSRII flow cytometer (BD Biosciences) and analyzed using the FCAP Array Software Version 3.0 (BD Biosciences).

Histopathology—Mice were infected as described with an inoculum size of ~5×10^7 or ~1×10^8 CFU. At 4 h and 8 h post-infection mice were euthanized with 3% isoflurane, and lungs were immediately inflated *in situ* with 1 ml of 10% buffered formalin (ThermoFisher Scientific) through a tracheal incision. Formalin-filled lungs were then tied at the trachea with a suture, excised, and stored in 25 ml of 10% formalin (ThermoFisher Scientific). Lungs were embedded in paraffin, sectioned, and stained with H&E by the University of Washington Histology and Imaging Core (Seattle, WA). Histopathological interpretation and scoring was performed by a veterinary pathologist who was blinded to mouse genetic background. Determination of the predominant lesion pattern was made following masked review of all sections. Three types of lesions were identified including: a) focal aggregation characterized by multiple distinct and highly cellular inflammatory foci, b) alveolar pattern with bacterial clusters distributed along alveolar walls, and c) mixed with both patterns represented equally. The degree of inflammatory cell and bacterial accumulations were

judged semi-quantitatively and assigned an all-inclusive ranking of severity from 1 (mild) to 4 (severe).

Alpha-toxin ELISA—Mouse lungs were extracted at 8 h post-infection and homogenized in 1 ml PBS containing 0.01% Triton X-100 and cOmplete Protease Inhibitor Cocktail (Roche). ELISAs were performed as previously described (Berube et al., 2014). MaxiSorp microtiter plates (Thermo-Fisher Scientific) were coated overnight at 4°C with 100 μg of 1μg ml^{-1} 7B8 monoclonal antibody to α-toxin in 0.2M Carbonate-Bicarbonate Buffer (pH = 9.4). Wells of coated plates were washed three times with 250 μl PBS-T (PBS containing 0.05% Tween-20 (Sigma-Aldrich)) before blocking for 1.5 h at room temperature with StartingBlock (PBS) buffer (Thermo-Fisher Scientific) containing 0.05% Tween-20 (Sigma-Aldrich). Lung homogenate and α-toxin standard was added at 100 μl per well and incubated for 1.5 h at room temperature. Wells were washed three times with 250 μl PBS-T. Rabbit anti-α-toxin polyclonal serum was added (diluted to 1:5000 in 100 μl PBS-T per well) and incubated for 1.5 h at room temperature. Wells washing was repeated three times, 100 μl of goat anti-rabbit IgG conjugated to HRP was added (diluted to 1:10000 in PBS-T), and the plate was incubated for 1.5 h at room temperature. A final set of three PBS-T washes was repeated before measuring HRP-signal with 1-Step Ultra TMB-ELISA substrate solution (Thermo-Fisher Scientific) at 450 nm.

QUANTIFICATION AND STATISTICAL ANALYSIS

Statistical method and sample size (n) for experiments are indicated in the corresponding figure legend. For all *in vitro* studies, n indicates the number of independent experiments. For *in vivo* studies, n indicates the number of mice per group. Statistical analysis was performed using Prism 6 Software (GraphPad) on the indicated biological replicates. A two-tailed Student's t test was performed on the means of parametric data and the Mann-Whitney U-test performed on the medians of non-parametric data. Statistical significance was defined as $p<0.05$. Error bars on figures show standard deviation.

KEY RESOURCES TABLE

The table highlights the genetically modified organisms and strains, cell lines, reagents, software, and source data **essential** to reproduce results presented in the manuscript. Depending on the nature of the study, this may include standard laboratory materials (i.e., food chow for metabolism studies), but the Table is **not** meant to be comprehensive list of all materials and resources used (e.g., essential chemicals such as SDS, sucrose, or standard culture media don't need to be listed in the Table). **Items in the Table must also be reported in the Method Details section within the context of their use.** The number of **primers and RNA sequences** that may be listed in the Table is restricted to no more than ten each. If there are more than ten primers or RNA sequences to report, please provide this information as a supplementary document and reference this file (e.g., See Table S1 for XX) in the Key Resources Table.

Please note that ALL references cited in the Key Resources Table ***must be included in the References list.*** Please report the information as follows:

- **REAGENT or RESOURCE:** Provide full descriptive name of the item so that it can be identified and linked with its description in the manuscript (e.g., provide version number for software, host source for antibody, strain name). In the Experimental Models section, please include all models used in the paper and describe each line/strain as: model organism: name used for strain/line in paper: genotype. (i.e., Mouse: $OXTR^{fl/fl}$: B6.129(SJL)-$Oxtr^{tm1.1Wsy/J}$). In the Biological Samples section, please list all samples obtained from commercial sources or biological repositories. Please note that software mentioned in the Methods Details or Data and Software Availability section needs to be also included in the table. See the sample Table at the end of this document for examples of how to report reagents.
- **SOURCE:** Report the company, manufacturer, or individual that provided the item or where the item can obtained (e.g., stock center or repository). For materials distributed by Addgene, please cite the article describing the plasmid and include "Addgene" as part of the identifier. If an item is from another lab, please include the name of the principal investigator and a citation if it has been previously published. If the material is being reported for the first time in the current paper, please indicate as "this paper." For software, please provide the company name if it is commercially available or cite the paper in which it has been initially described.
- **IDENTIFIER:** Include catalog numbers (entered in the column as "Cat#" followed by the number, e.g., Cat#3879S). Where available, please include unique entities such as RRIDs, Model Organism Database numbers, accession numbers, and PDB or CAS IDs. For antibodies, if applicable and available, please also include the lot number or clone identity. For software or data resources, please include the URL where the resource can be downloaded. Please ensure accuracy of the identifiers, as they are essential for generation of hyperlinks to external sources when available. Please see the Elsevier list of Data Repositories with automated bidirectional linking for details. When listing more than one identifier for the same item, use semicolons to separate them (e.g. Cat#3879S; RRID: AB_2255011). If an identifier is not available, please enter "N/A" in the column.
  - ***A NOTE ABOUT RRIDs:*** We highly recommend using RRIDs as the identifier (in particular for antibodies and organisms, but also for software tools and databases). For more details on how to obtain or generate an RRID for existing or newly generated resources, please visit the RII or search for RRIDs.

Please use the empty table that follows to organize the information in the sections defined by the subheading, skipping sections not relevant to your study. Please do not add subheadings. To add a row, place the cursor at the end of the row above where you would like to add the row, just outside the right border of the table. Then press the ENTER key to add the row. You do not need to delete empty rows. Each entry must be on a separate row; do not list

multiple items in a single table cell. Please see the sample table at the end of this document for examples of how reagents should be cited.

TABLE FOR AUTHOR TO COMPLETE

Please upload the completed table as a separate document. **Please do not add subheadings to the** Key Resources Table. If you wish to make an entry that does not fall into one of the subheadings below, please contact your handling editor. (**NOTE:** For authors publishing in Current Biology, please note that references within the KRT should be in numbered style, rather than Harvard.)

KEY RESOURCES TABLE

REAGENT or RESOURCE	SOURCE	IDENTIFIER
Antibodies		
Anti-HA mouse IgG1, clone 16B12, Alexa Fluor 488 Conjugate	Molecular Probes	Cat#A21287; RRID: AB_2535829
Anti-HA mouse antibody, monoclonal HA-7	Sigma-Aldrich	Cat#H3663; RRID: AB_262051
7B8 monoclonal antibody to α-toxin	Berube et al., 2014	N/A
Rabbit anti-α-toxin polyclonal serum	Berube et al., 2014	N/A
Anti-rabbit goat IgG HRP conjugate	ThermoFisher Sci	Cat#65-6120; RRID: AB_2533967
Bacterial and Virus Strains		
Staphylococcus aureus HG003; NCTC8325 derivative	Herbert et al., 2010	RU083
HG003 Δ*agrA*	This paper	RU111
HG003 Δ*agrC*	This paper	RU141
HG003 *agrC* C91S C371S	This paper	RU161
HG003 + pEPSA5	This paper	RU170
HG003 Δ*agrA* + pEPSA5	This paper	RU171
HG003 Δ*agrA* + p*agrA*	This paper	RU174
HG003 Δ*agrA* + p*agrA* C6V	This paper	RU487
HG003 Δ*agrA* + p*agrA* C55S	This paper	RU497
HG003 Δ*agrA* + p*agrA* C123N	This paper	RU494
HG003 Δ*agrA* + p*agrA* C199S	This paper	RU475
HG003 Δ*agrA* + p*agrA-HA*	This paper	RU198
HG003 Δ*agrA* + p*agrAC55SC199S-HA*	This paper	RU551
HG003 C-terminus HA-tagged *agrA* (chromosomal)	This paper	RU226
HG003 Δ*agrBD*	This paper	RU299
HG003 Δ*sarA*	This paper	RU536
Staphylococcus aureus Newman Strep^R	This paper	RU371
Newman Δ*agrC* Strep^R	This paper	RU373
Newman Δ*agrA* Strep^R	This paper	RU498
Newman *agrA* C55S C199S Strep^R	This paper	RU516

REAGENT or RESOURCE	SOURCE	IDENTIFIER
S. aureus SF8300	Diep et al., 2008	RU078
S. aureus JE2	BEI Resources	FLS318
S. aureus JE2 *sarU*::Tn (transposon mutant)	BEI Resources	RU359
S. aureus RN4220; NCTC8325 derivative, restriction deficient cloning host	Kreiswirth et al., 1983	RU062
E. coli ElectroMAX DH10B; F⁻*mcr*A Δ(*mrr-hsd*RMS-*mcr*BC) Φ80*lac*ZΔM15 Δ*lac*X74 *rec*A1 *end*A1*ara*D139Δ(*ara*, *leu*)7697 *gal*U *gal*K λ⁻*rps*L *nup*G	Invitrogen	Cat#18290015
DH10B + pIMAY	Monk et al., 2012	RU097
DH10B + pIMAYΔ*agrA*	This paper	RU127
DH10B + pIMAYΔ*agrC*	This paper	RU146
DH10B + pIMAY*agrA-HA*	This paper	RU218
DH10B + pIMAYΔ*sarA*	This paper	RU155
DH5α + pEPSA5	Forsyth et al., 2002	RU133
DH10B + p*agrA-HA*	This paper	RU194
DH10B + p*agrAC55SC199S-HA*	This paper	RU549
Biological Samples		
Chemicals, Peptides, and Recombinant Proteins		
Lysostaphin	AMBI Products	Cat#LSPN-50
DEA NONOate	Cayman Chemicals	Cat#82100
PAPA NONOate	Cayman Chemicals	Cat#82140
Alpha-Toxin	Berube et al. 2014	N/A
Streptavidin, Alexa Fluor 647 Conjugate	Molecular Probes	Cat#S32357
Critical Commercial Assays		
QuikChange Lightning Site-Directed Mutagenesis Kit	Agilent Technologies	Cat#210518-5
Dynabeads M-280 Sheep anti-Mouse IgG	Novex	Cat#11201D
Pierce Anti-HA Magnetic Beads	ThermoFisher Scientific	Cat#88836
EZ-Link HPDP-Biotin	ThermoFisher Scientific	Cat#21341
BD Cytometric Bead Array Mouse/Rat Soluble Protein Master Buffer Kit	BD Biosciences	Cat#558266
BD Cytometric Bead Array Mouse Enhanced Sensitivity Master Buffer Kit	BD Biosciences	Cat#562246
Deposited Data		
Experimental Models: Cell Lines		

REAGENT or RESOURCE	SOURCE	IDENTIFIER
Experimental Models: Organisms/Strains		
C57BL/6J SPF mice	Jackson Laboratory	Cat#000664
B6.129P2-*Nos2*^{tm1Lau}/J SPF mice	Jackson Laboratory	Cat#002609
Oligonucleotides		
Primers for cloning, mutagenesis, and qPCR, See Table S2		
Recombinant DNA		
pIMAY	Monk et al., 2012	N/A
pIMAYΔ*agrA*	This paper	N/A
pIMAY*agrA* C55S C199S	This paper	N/A
pIMAYΔ*agrC*	This paper	N/A
pIMAY*agrC* C91S C371S	This paper	N/A
pIMAY*agrA-HA*	This paper	N/A
pIMAYΔ*sarA*	This paper	N/A
pEPSA5	Forsyth et al., 2002	N/A
p*agrA*	This paper	N/A
p*agrA* C6V	This paper	N/A
p*agrA* C55S	This paper	N/A
p*agrA* C123N	This paper	N/A
p*agrA* C199S	This paper	N/A
p*agrA-HA*	This paper	N/A
p*agrAC55SC199S-HA*	This paper	N/A
Software and Algorithms		
Clustal Omega Multiple Sequence Alignment	Sievers et al., 2011	http://www.ebi.ac.uk/Tools/msa/clustalo/
FCAP Array Software Version 3.0	BD Bioscience	Cat#652099
ImageJ Version 1.47 Software	Wayne Rasband, U. S. National Institutes of Health	https://imagej.nih.gov/ij/
MacVector Version 12. 0. 3	MacVector, Inc	http://macvector.com/index.html
Phyre2	Kelley et al., 2015	http://www.sbg.bio.ic.ac.uk/phyre2/html/page.cgi?id=index
PyMOL Molecular Graphics System Version 1.8	S Schrödinger, LLC	https://www.pymol.org/
Prism 6 Software	GraphPad	https://www.graphpad.com/
Scaffold Version 4. 0. 4	Proteome Software	http://www.proteomesoftware.com/
Sorcerer Sequest	Sage-N Research, Inc	https://www.sagenresearch.com/
Other		

TABLE WITH EXAMPLES FOR AUTHOR REFERENCE

REAGENT or RESOURCE	SOURCE	IDENTIFIER
Antibodies		
Rabbit monoclonal anti-Snail	Cell Signaling Technology	Cat#3879S; RRID: AB_225501
Mouse monoclonal anti-Tubulin (clone DM1A)	Sigma-Aldrich	Cat#T9026; RRID: AB_477593
Rabbit polyclonal anti-BMAL1	This paper	N/A
Bacterial and Virus Strains		
pAAV-hSyn-DIO-hM3D(Gq)-mCherry	Krashes et al., 2011	Addgene AAV5; 44361-AAV5
AAV5-EF1a-DIO-hChR2(H134R)-EYFP	Hope Center Viral Vectors Core	N/A
Cowpox virus Brighton Red	BEI Resources	NR-88
Zika-SMGC-1, GENBANK: KX266255	Isolated from patient (Wang et al., 2016)	N/A
Staphylococcus aureus	ATCC	ATCC 29213
Streptococcus pyogenes: M1 serotype strain: strain SF370; M1 GAS	ATCC	ATCC 700294
Biological Samples		
Healthy adult BA9 brain tissue	University of Maryland Brain & Tissue Bank; http://medschool.umaryland.edu/btbank/	Cat#UMB1455
Human hippocampal brain blocks	New York Brain Bank	http://nybb.hs.columbia.edu/
Patient-derived xenografts (PDX)	Children's Oncology Group Cell Culture and Xenograft Repository	http://cogcell.org/
Chemicals, Peptides, and Recombinant Proteins		
MK-2206 AKT inhibitor	Selleck Chemicals	S1078; CAS: 1032350-13-2
SB-505124	Sigma-Aldrich	S4696; CAS: 694433-59-5 (free
Picrotoxin	Sigma-Aldrich	P1675; CAS: 124-87-8
Human TGF-β	R&D	240-B; GenPept: P01137
Activated S6K1	Millipore	Cat#14-486
GST-BMAL1	Novus	Cat#H00000406-P01
Critical Commercial Assays		
EasyTag EXPRESS 35S Protein Labeling Kit	Perkin-Elmer	NEG772014MC
CaspaseGlo 3/7	Promega	G8090
TruSeq ChIP Sample Prep Kit	Illumina	IP-202-1012
Deposited Data		
Raw and analyzed data	This paper	GEO: GSE63473
B-RAF RBD (apo) structure	This paper	PDB: 5J17
Human reference genome NCBI build 37, GRCh37	Genome Reference Consortium	http://www.ncbi.nlm.nih.gov/pro
Nanog STILT inference	This paper; Mendeley Data	http://dx.doi.org/10.17632/wx6s
Affinity-based mass spectrometry performed with 57 genes	This paper; and Mendeley Data	Table S8; http://dx.doi.org/10.17
Experimental Models: Cell Lines		
Hamster: CHO cells	ATCC	CRL-11268

REAGENT or RESOURCE	SOURCE	IDENTIFIER
D. melanogaster: Cell line S2: S2-DRSC	Laboratory of Norbert Perrimon	FlyBase: FBtc0000181
Human: Passage 40 H9 ES cells	MSKCC stem cell core facility	N/A
Human: HUES 8 hESC line (NIH approval number NIHhESC-09-0021)	HSCI iPS Core	hES Cell Line: HUES-8
Experimental Models: Organisms/Strains		
C. elegans: Strain BC4011: srl-1(s2500) II; dpy-18(e364) III; unc-46(e177)rol-3(s1040) V.	Caenorhabditis Genetics Center	WB Strain: BC4011; WormBase
D. melanogaster: RNAi of Sxl: y[1] sc[*] v[1]; P{TRiP.HMS00609}attP2	Bloomington Drosophila Stock Center	BDSC:34393; FlyBase: FBtp00
S. cerevisiae: Strain background: W303	ATCC	ATTC: 208353
Mouse: R6/2: B6CBA-Tg(HDexon1)62Gpb/3J	The Jackson Laboratory	JAX: 006494
Mouse: OXTRfl/fl: B6.129(SJL)-Oxtr$^{tm1.1Wsy}$/J	The Jackson Laboratory	RRID: IMSR_JAX:008471
Zebrafish: Tg(Shha:GFP)t10: t10Tg	Neumann and Nuesslein-Volhard, 2000	ZFIN: ZDB-GENO-060207-1
Arabidopsis: 35S::PIF4-YFP, BZR1-CFP	Wang et al., 2012	N/A
Arabidopsis: JYB1021.2: pS24(AT5G58010)::cS24:GFP(-G):NOS #1	NASC	NASC ID: N70450
Oligonucleotides		
siRNA targeting sequence: PIP5K I alpha #1: ACACAGUACUCAGUUGAUA	This paper	N/A
Primers for XX, see Table SX	This paper	N/A
Primer: GFP/YFP/CFP Forward: GCACGACTTCTTCAAGTCCGCCATGCC	This paper	N/A
Morpholino: MO-pax2a GGTCTGCTTTGCAGTGAATATCCAT	Gene Tools	ZFIN: ZDB-MRPHLNO-06110
ACTB (hs01060665_g1)	Life Technologies	Cat#4331182
RNA sequence: hnRNPA1_ligand: UAGGGACUUAGGGUUCUCUCUAGGGACUUAGGGUUCUCUCUAGGGA	This paper	N/A
Recombinant DNA		
pLVX-Tight-Puro (TetOn)	Clonetech	Cat#632162
Plasmid: GFP-Nito	This paper	N/A
cDNA GH111110	Drosophila Genomics Resource Center	DGRC:5666; FlyBase:FBcl013
AAV2/1-hsyn-GCaMP6- WPRE	Chen et al., 2013	N/A
Mouse raptor: pLKO mouse shRNA 1 raptor	Thoreen et al., 2009	Addgene Plasmid #21339
Software and Algorithms		
Bowtie2	Langmead and Salzberg, 2012	http://bowtie-bio.sourceforge.ne
Samtools	Li et al., 2009	http://samtools.sourceforge.net/
Weighted Maximal Information Component Analysis v0.9	Rau et al., 2013	https://github.com/ChristophRau
ICS algorithm	This paper; Mendeley Data	http://dx.doi.org/10.17632/5hvp
Other		
Sequence data, analyses, and resources related to the ultra-deep sequencing of the AML31 tumor, relapse, and matched normal.	This paper	http://aml31.genome.wustl.edu
Resource website for the AML31 publication	This paper	https://github.com/chrisamiller/a

Supplementary Material

Refer to Web version on PubMed Central for supplementary material.

Acknowledgments

The authors thank Donna Prunkard at the University of Washington Pathology Flow Cytometry Core for assistance with flow cytometer setup. We thank An Dowon for assistance with histology sample preparation. We also thank Juliane Bubeck-Wardenburg and Bryan J. Berube for providing reagents and protocols for α-toxin ELISAs. This work was supported by NIH grants T32 AI55396 (R.U), AI39557 (F.C.F), and AI123124 (F.C.F).

References

Bang IS, Liu L, Vazquez-Torres A, Crouch ML, Stamler JS, Fang FC. Maintenance of nitric oxide and redox homeostasis by the *Salmonella* flavohemoglobin Hmp. J Biol Chem. 2006; 281:28039–28047. [PubMed: 16873371]

Bartlett AH, Foster TJ, Hayashida A, Park PW. Alpha-toxin facilitates the generation of CXC chemokine gradients and stimulates neutrophil homing in *Staphylococcus aureus* pneumonia. Journal of Infectious Diseases. 2008; 198:1529–1535. [PubMed: 18823272]

Bast DJ, Yue M, Chen X, Bell D, Dresser L, Saskin R, Mandell LA, Low DE, de Azavedo JCS. Novel murine model of pneumococcal pneumonia: use of temperature as a measure of disease severity to compare the efficacies of moxifloxacin and levofloxacin. Antimicrob Agents Chemother. 2004; 48:3343–3348. [PubMed: 15328095]

Berube BJ, Sampedro GR, Otto M, Wardenburg JB. The *psma* locus regulates production of *Staphylococcus aureus* alpha-toxin during infection. Infect Immun. 2014; 82:3350–3358. [PubMed: 24866799]

Bogdan C. Nitric oxide synthase in innate and adaptive immunity: an update. Trends in Immunology. 2015; 36:161–178. [PubMed: 25687683]

Boisset S, Geissmann T, Huntzinger E, Fechter P, Bendridi N, Possedko M, Chevalier C, Helfer AC, Benito Y, Jacquier A, et al. *Staphylococcus aureus* RNAIII coordinately represses the synthesis of virulence factors and the transcription regulator Rot by an antisense mechanism. Genes & Development. 2007; 21:1353–1366. [PubMed: 17545468]

Bubeck Wardenburg J, Bae T, Otto M, Deleo FR, Schneewind O. Poring over pores: alpha-hemolysin and Panton-Valentine leukocidin in *Staphylococcus aureus* pneumonia. Nat Med. 2007a; 13:1405–1406. [PubMed: 18064027]

Bubeck Wardenburg J, Patel RJ, Schneewind O. Surface proteins and exotoxins are required for the pathogenesis of *Staphylococcus aureus* pneumonia. Infect Immun. 2007b; 75:1040–1044. [PubMed: 17101657]

Burian M, Wolz C, Goerke C. Regulatory adaptation of *Staphylococcus aureus* during nasal colonization of humans. Plos One. 2010; 5:e10040. [PubMed: 20386721]

Crane BR, Sudhamsu J, Patel BA. Bacterial nitric oxide synthases. Annu Rev Biochem. 2010; 79:445–470. [PubMed: 20370423]

Diep BA, Palazzolo-Ballance AM, Tattevin P, Basuino L, Braughton KR, Whitney AR, Chen L, Kreiswirth BN, Otto M, DeLeo FR, Chambers HF. Contribution of Panton-Valentine leukocidin in community-associated methicillin-resistant *Staphylococcus aureus* pathogenesis. Plos One. 2008; 3:e3198. [PubMed: 18787708]

Domingos P, Prado AM, Wong A, Gehring C, Feijo JA. Nitric oxide: a multitasked signaling gas in plants. Mol Plant. 2015; 8:506–520. [PubMed: 25680232]

Doulias PT, Greene JL, Greco TM, Tenopoulou M, Seeholzer SH, Dunbrack RL, Ischiropoulos H. Structural profiling of endogenous S-nitrosocysteine residues reveals unique features that accommodate diverse mechanisms for protein S-nitrosylation. Proc Natl Acad Sci U S A. 2010; 107:16958–16963. [PubMed: 20837516]

Fang FC. Antimicrobial reactive oxygen and nitrogen species: Concepts and controversies. Nature Reviews Microbiology. 2004; 2:820–832. [PubMed: 15378046]

Fang, FC. Nitric Oxide and Infection. New York: Kluwer Academic/Plenum Publishers; 1999.

Forsyth RA, Haselbeck RJ, Ohlsen KL, Yamamoto RT, Xu H, Trawick JD, Wall D, Wang L, Brown-Driver V, Froelich JM, et al. A genome-wide strategy for the identification of essential genes in *Staphylococcus aureus*. Mol Microbiol. 2002; 43:1387–1400. [PubMed: 11952893]

Frank KM, Zhou T, Moreno-Vinasco L, Hollett B, Garcia JG, Bubeck Wardenburg J. Host response signature to *Staphylococcus aureus* alpha-hemolysin implicates pulmonary Th17 response. Infect Immun. 2012; 80:3161–3169. [PubMed: 22733574]

Förstermann U, Sessa WC. Nitric oxide synthases: regulation and function. Eur Heart J. 2012; 33:829–837. 837a–837d. [PubMed: 21890489]

Galperin MY. Telling bacteria: do not LytTR. Structure. 2008; 16:657–659. [PubMed: 18462668]

Goerke C, Campana S, Bayer MG, Döring G, Botzenhart K, Wolz C. Direct quantitative transcript analysis of the agr regulon of *Staphylococcus aureus* during human infection in comparison to the expression profile in vitro. Infect Immun. 2000; 68:1304–1311. [PubMed: 10678942]

Hall PR, Elmore BO, Spang CH, Alexander SM, Manifold-Wheeler BC, Castleman MJ, Daly SM, Peterson MM, Sully EK, Femling JK, et al. Nox2 modification of LDL is essential for optimal apolipoprotein B-mediated control of *agr* type III *Staphylococcus aureus* quorum-sensing. Plos Pathogens. 2013; 9:e1003166. [PubMed: 23459693]

Herbert S, Ziebandt AK, Ohlsen K, Schäfer T, Hecker M, Albrecht D, Novick R, Götz F. Repair of global regulators in *Staphylococcus aureus* 8325 and comparative analysis with other clinical isolates. Infect Immun. 2010; 78:2877–2889. [PubMed: 20212089]

Hirschhausen N, Schlesier T, Peters G, Heilmann C. Characterization of the modular design of the autolysin/adhesin Aaa from *Staphylococcus aureus*. Plos One. 2012; 7:e40353. [PubMed: 22768285]

Hussell T, Bell TJ. Alveolar macrophages: plasticity in a tissue-specific context. Nat Rev Immunol. 2014; 14:81–93. [PubMed: 24445666]

Jaffrey SR, Snyder SH. The biotin switch method for the detection of *S*-nitrosylated proteins. Sci STKE. 2001; 2001:pl1.

James EH, Edwards AM, Wigneshweraraj S. Transcriptional downregulation of *agr* expression in *Staphylococcus aureus* during growth in human serum can be overcome by constitutively active mutant forms of the sensor kinase AgrC. FEMS Microbiol Lett. 2013; 349:153–162. [PubMed: 24164684]

Karlinsey JE, Bang IS, Becker LA, Frawley ER, Porwollik S, Robbins HF, Thomas VC, Urbano R, McClelland M, Fang FC. The NsrR regulon in nitrosative stress resistance of *Salmonella enterica* serovar Typhimurium. Molecular Microbiology. 2012; 85:1179–1193. [PubMed: 22831173]

Kelley LA, Mezulis S, Yates CM, Wass MN, Sternberg MJE. The Phyre2 web portal for protein modeling, prediction and analysis. Nat Protoc. 2015; 10:845–858. [PubMed: 25950237]

Kinkel TL, Roux CM, Dunman PM, Fang FC. The *Staphylococcus aureus* SrrAB two-Component system promotes resistance to nitrosative stress and hypoxia. Mbio. 2013; 4:e00696–00613. [PubMed: 24222487]

Kitur K, Parker D, Nieto P, Ahn DS, Cohen TS, Chung S, Wachtel S, Bueno S, Prince A. Toxin-induced necroptosis is a major mechanism of *Staphylococcus aureus* lung damage. Plos Pathogens. 2015; 11:e1004820. [PubMed: 25880560]

Kopf M, Schneider C, Nobs SP. The development and function of lung-resident macrophages and dendritic cells. Nat Immunol. 2015; 16:36–44. [PubMed: 25521683]

Kreiswirth BN, Löfdahl S, Betley MJ, O'Reilly M, Schlievert PM, Bergdoll MS, Novick RP. The toxic shock syndrome exotoxin structural gene is not detectably transmitted by a prophage. Nature. 1983; 305:709–712. [PubMed: 6226876]

Köhler J, Breitbach K, Renner C, Heitsch AK, Bast A, van Rooijen N, Vogelgesang S, Steinmetz I. NADPH-oxidase but not inducible nitric oxide synthase contributes to resistance in a murine *Staphylococcus aureus* Newman pneumonia model. Microbes Infect. 2011; 13:914–922. [PubMed: 21635963]

Li C, Li H, Jiang Z, Zhang T, Wang Y, Li Z, Wu Y, Ji S, Xiao S, Ryffel B, et al. Interleukin-33 increases antibacterial defense by activation of inducible nitric oxide synthase in skin. Plos Pathogens. 2014; 10:e1003918. [PubMed: 24586149]

li L, Pian Y, Chen S, Hao H, Zheng Y, Zhu L, Xu B, Liu K, Li M, Jiang H, et al. Phenol-soluble modulin α4 mediates *Staphylococcus aureus*-associated vascular leakage by stimulating heparin-binding protein release from neutrophils. Scientific Reports. 2016; 6:29373. [PubMed: 27383625]

Lundberg JO, Farkas-Szallasi T, Weitzberg E, Rinder J, Lidholm J, Anggård A, Hökfelt T, Lundberg JM, Alving K. High nitric oxide production in human paranasal sinuses. Nat Med. 1995; 1:370–373. [PubMed: 7585069]

MacMicking J, Xie QW, Nathan C. Nitric oxide and macrophage function. Annual Review of Immunology. 1997; 15:323–350.

Manifold-Wheeler BC, Elmore BO, Triplett KD, Castleman MJ, Otto M, Hall PR. Serum lipoproteins are critical for pulmonary innate defense against *Staphylococcus aureus* quorum sensing. The Journal of Immunology. 2016; 196:328–335. [PubMed: 26608923]

Martin FJ, Parker D, Harfenist BS, Soong G, Prince A. Participation of CD11c(+) leukocytes in methicillin-resistant *Staphylococcus aureus* clearance from the lung. Infect Immun. 2011; 79:1898–1904. [PubMed: 21402768]

McInnes IB, Leung B, Wei XQ, Gemmell CC, Liew FY. Septic arthritis following *Staphylococcus aureus* infection in mice lacking inducible nitric oxide synthase. Journal of Immunology. 1998; 160:308–315.

Merrikh CN, Brewer BJ, Merrikh H. The *B. subtilis* accessory helicase PcrA facilitates DNA replication through transcription units. PLoS Genet. 2015; 11:e1005289. [PubMed: 26070154]

Monk IR, Shah IM, Xu M, Tan MW, Foster TJ. Transforming the untransformable: application of direct transformation to manipulate genetically *Staphylococcus aureus* and *Staphylococcus epidermidis*. MBio. 2012; 3:e00277. [PubMed: 22434850]

Morfeldt E, Taylor D, von Gabain A, Arvidson S. Activation of alpha-toxin translation in *Staphylococcus aureus* by the trans-encoded antisense RNA, RNAIII. EMBO J. 1995; 14:4569–4577. [PubMed: 7556100]

Novick RP. Genetic systems in staphylococci. Methods Enzymol. 1991; 204:587–636. [PubMed: 1658572]

Novick RP, Geisinger E. Quorum sensing in staphylococci. Annu Rev Genet. 2008; 42:541–564. [PubMed: 18713030]

Parker D, Ryan CL, Alonzo F, Torres VJ, Planet PJ, Prince A. CD4(+) T cells promote the pathogenesis of *Staphylococcus aureus* pneumonia. Journal of Infectious Diseases. 2015; 211:835–845. [PubMed: 25240171]

Peterson MM, Mack JL, Hall PR, Alsup AA, Alexander SM, Sully EK, Sawires YS, Cheung AL, Otto M, Gresham HD. Apolipoprotein B is an innate barrier against invasive *Staphylococcus aureus* infection. Cell Host & Microbe. 2008; 4:555–566. [PubMed: 19064256]

Plate L, Marletta MA. Nitric oxide-sensing H-NOX proteins govern bacterial communal behavior. Trends in Biochemical Sciences. 2013; 38:566–575. [PubMed: 24113192]

Qiu R, Pei W, Zhang L, Lin J, Ji G. Identification of the putative staphylococcal AgrB catalytic residues involving the proteolytic cleavage of AgrD to generate autoinducing peptide. J Biol Chem. 2005; 280:16695–16704. [PubMed: 15734745]

Queck SY, Jameson-Lee M, Villaruz AE, Bach TH, Khan BA, Sturdevant DE, Ricklefs SM, Li M, Otto M. RNAIII-independent target gene control by the agr quorum-sensing system: insight into the evolution of virulence regulation in *Staphylococcus aureus*. Mol Cell. 2008; 32:150–158. [PubMed: 18851841]

Richardson AR, Dunman PM, Fang FC. The nitrosative stress response of *Staphylococcus aureus* is required for resistance to innate immunity. Molecular Microbiology. 2006; 61:927–939. [PubMed: 16859493]

Richardson AR, Libby SJ, Fang FC. A nitric oxide-inducible lactate dehydrogenase enables *Staphylococcus aureus* to resist innate immunity. Science. 2008; 319:1672–1676. [PubMed: 18356528]

Richardson AR, Payne EC, Younger N, Karlinsey JE, Thomas VC, Becker LA, Navarre WW, Castor ME, Libby SJ, Fang FC. Multiple targets of nitric oxide in the tricarboxylic acid cycle of *Salmonella enterica* serovar Typhimurium. Cell Host & Microbe. 2011; 10:33–43. [PubMed: 21767810]

Robertson CM, Perrone EE, McConnell KW, Dunne WM, Boody B, Brahmbhatt T, Diacovo MJ, Van Rooijen N, Hogue LA, Cannon CL, et al. Neutrophil depletion causes a fatal defect in murine pulmonary *Staphylococcus aureus* clearance. J Surg Res. 2008; 150:278–285. [PubMed: 18621398]

Rothfork JM, Timmins GS, Harris MN, Chen X, Lusis AJ, Otto M, Cheung AL, Gresham HD. Inactivation of a bacterial virulence pheromone by phagocyte-derived oxidants: New role for the NADPH oxidase in host defense. Proceedings of the National Academy of Sciences of the United States of America. 2004; 101:13867–13872. [PubMed: 15353593]

Sasaki S, Miura T, Nishikawa S, Yamada K, Hirasue M, Nakane A. Protective role of nitric oxide in *Staphylococcus aureus* infection in mice. Infection and Immunity. 1998; 66:1017–1022. [PubMed: 9488390]

Schmittgen TD, Livak KJ. Analyzing real-time PCR data by the comparative C(T) method. Nat Protoc. 2008; 3:1101–1108. [PubMed: 18546601]

Sidote DJ, Barbieri CM, Wu T, Stock AM. Structure of the *Staphylococcus aureus* AgrA LytTR domain bound to DNA reveals a beta fold with an unusual mode of binding. Structure. 2008; 16:727–735. [PubMed: 18462677]

Sievers F, Wilm A, Dineen D, Gibson TJ, Karplus K, Li W, Lopez R, McWilliam H, Remmert M, Söding J, et al. Fast, scalable generation of high-quality protein multiple sequence alignments using Clustal Omega. Mol Syst Biol. 2011; 7:539. [PubMed: 21988835]

Spiro S. Regulators of bacterial responses to nitric oxide. Fems Microbiology Reviews. 2007; 31:193–211. [PubMed: 17313521]

Stamler JS, Lamas S, Fang FC. Nitrosylation: The prototypic redox-based signaling mechanism. Cell. 2001; 106:675–683. [PubMed: 11572774]

Sun F, Liang H, Kong X, Xie S, Cho H, Deng X, Ji Q, Zhang H, Alvarez S, Hicks LM, et al. Quorum-sensing *agr* mediates bacterial oxidation response via an intramolecular disulfide redox switch in the response regulator AgrA. Proceedings of the National Academy of Sciences of the United States of America. 2012; 109:9095–9100. [PubMed: 22586129]

Thammavongsa V, Kim HK, Missiakas D, Schneewind O. Staphylococcal manipulation of host immune responses. Nature Reviews Microbiology. 2015; 13:529–543. [PubMed: 26272408]

Theis T, Skurray RA, Brown MH. Identification of suitable internal controls to study expression of a *Staphylococcus aureus* multidrug resistance system by quantitative real-time PCR. J Microbiol Methods. 2007; 70:355–362. [PubMed: 17590462]

Thoendel M, Horswill AR. Identification of *Staphylococcus aureus* AgrD residues required for autoinducing peptide biosynthesis. Journal of Biological Chemistry. 2009; 284:21828–21838. [PubMed: 19520867]

Thoendel M, Horswill AR. Random mutagenesis and topology analysis of the autoinducing peptide biosynthesis proteins in *Staphylococcus aureus*. Mol Microbiol. 2012; 87:318–337. [PubMed: 23216863]

Thoendel M, Kavanaugh JS, Flack CE, Horswill AR. Peptide signaling in the Staphylococci. Chemical Reviews. 2011; 111:117–151. [PubMed: 21174435]

van den Berg S, Laman JD, Boon L, ten Kate MT, de Knegt GJ, Verdijk RM, Verbrugh HA, Nouwen JL, Bakker-Woudenberg IAJM. Distinctive cytokines as biomarkers predicting fatal outcome of severe *Staphylococcus aureus* bacteremia in mice. Plos One. 2013; 8:e59107. [PubMed: 23520553]

Vitko NP, Spahich NA, Richardson AR. Glycolytic dependency of high-level nitric oxide resistance and virulence in *Staphylococcus aureus*. Mbio. 2015; 6:e00045. [PubMed: 25852157]

Yang Z, Huang YCT, Koziel H, de Crom R, Ruetten H, Wohlfart P, Thomsen RW, Kahlert JA, Sørensen HT, Jozefowski S, et al. Female resistance to pneumonia identifies lung macrophage nitric oxide synthase-3 as a therapeutic target. Elife. 2014; 3:e03711.

Highlights

- Nitric oxide binds to the staphylococcal virulence regulator AgrA
- *S*-nitrosylation of AgrA inhibits staphylococcal virulence
- Nitric oxide is protective in a murine pneumonia model
- Nitric oxide functions as an anti-virulence innate immunity factor

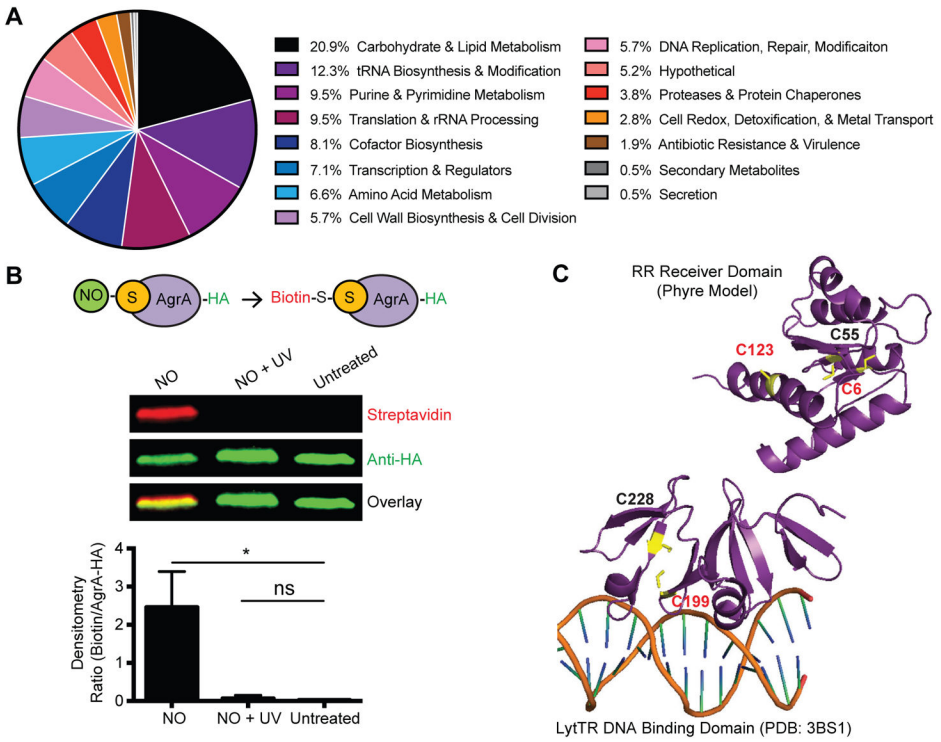

Figure 1. Mass Spectrometry-based Proteomic Analysis Identifies AgrA Virulence Regulator as a Target of *S*-nitrosylation

(A) Summary of identified NO-modified proteins categorized by biological pathway.

(B) Biotin switch validation of AgrA cysteines as NO targets. Representative immunoprecipitation-western blot (top, n=3) probed with streptavidin and anti-HA antibody to detect biotinylation and HA-tagged AgrA, respectively. Densitometry of three independent experiments (bottom) quantifying the ratio of biotin to AgrA. Data are represented as means with error bars showing standard deviation. UV, ultraviolet light. Student's t test, *p<0.05; ns, not significant.

(C) AgrA cysteine residues in the RR receiver domain (top) and LytTR DNA binding domain (bottom). *S*-nitrosylation of C6, C123, and C199 (red) was detected by mass spectrometry.

See also Figure S1 and Table S1.

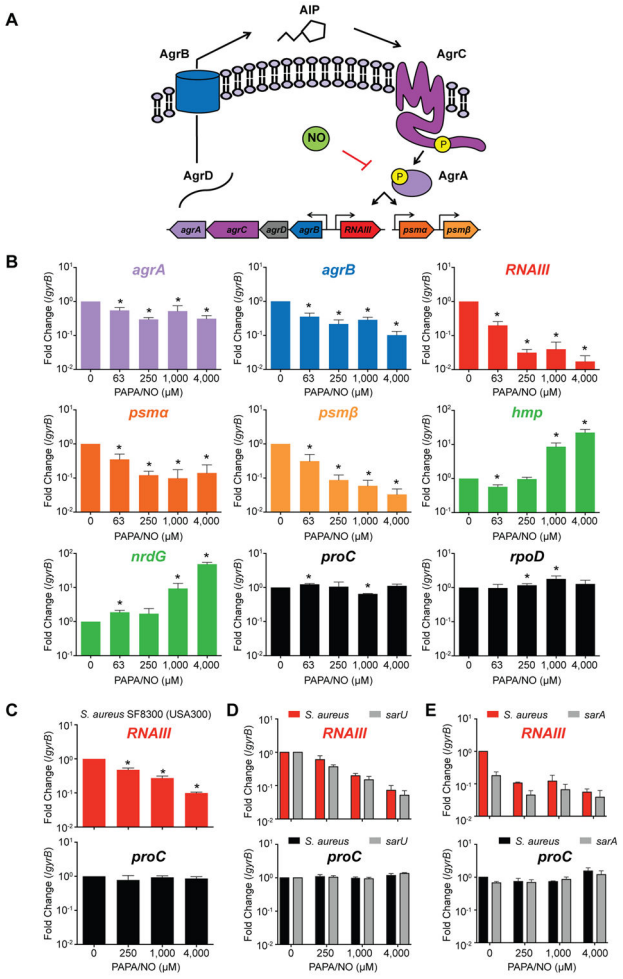

Figure 2. Nitric Oxide Inhibits Transcription of the *agr* Quorum Sensing Operon and AgrA-Regulated Virulence Factors

(A) Model of Agr quorum sensing and NO inhibition.

(B) RT-qPCR from *S. aureus* HG003 cultures (n=4) treated with increasing concentrations of the NO donor PAPA/NO. Agr-regulated genes include *agrA*, *agrB*, *RNAIII*, *psma* and *psmβ*; nitrosative stress-induced genes (green) include *hmp* and *nrdG*; control genes (black) include housekeeping genes *rpoD* and *proC*.

(C) RT-qPCR from *S. aureus* SF8300 cultures (n=3).

(D) RT-qPCR from cultures of *S. aureus* JE2 and its derived mutant with a transposon insertion in *sarU* (n=3).

(E) RT-qPCR from cultures of *S. aureus* HG003 and the derived *sarA* null mutant.

Student's t test, **p*<0.05.

For (B) through (E) data are represented as means with error bars showing standard deviation.

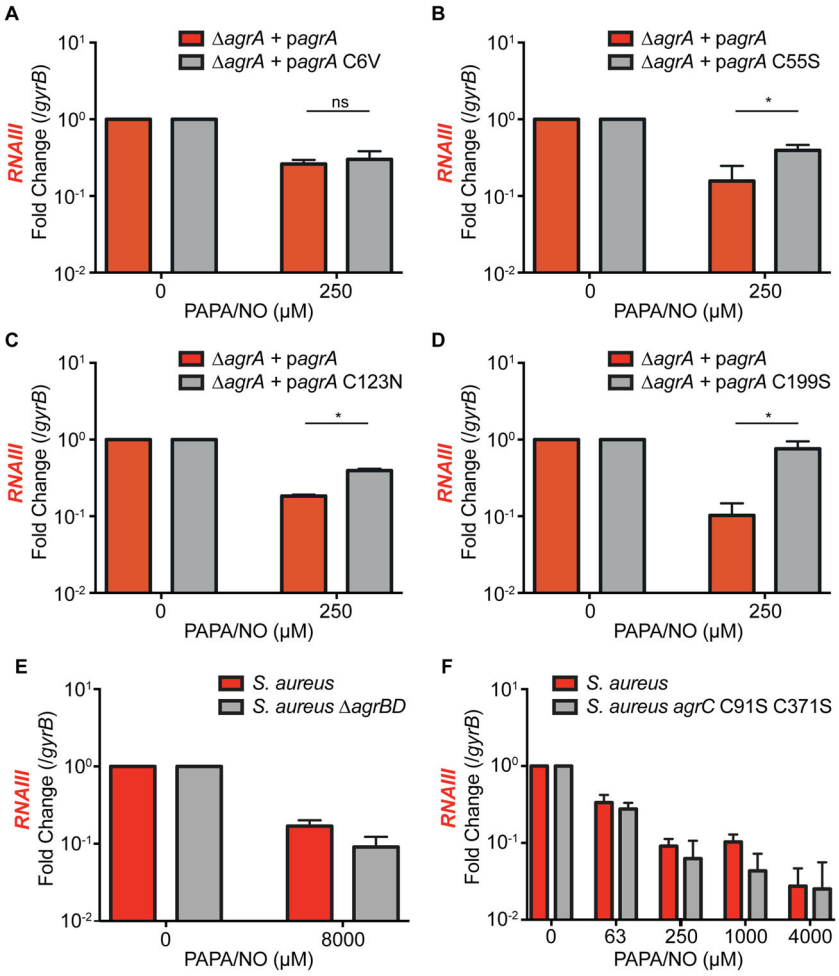

Figure 3. Nitric Oxide Inhibition of QS is Mediated by AgrA C55, C123, and C199

(A–D) RT-qPCR of *RNAIII* in PAPA/NO-treated *S. aureus* cultures (n=3) ectopically expressing AgrA alleles with single site-specific mutations (C6V, C55S, C123N, or C199S). Student's t test, *$p<0.05$; ns, not significant.

(E) RT-qPCR of *RNAIII* in an AIP biosynthesis mutant lacking *agrBD* after stimulation with 20% spent medium from wild-type *S. aureus* and treated with PAPA/NO (n=3).

(F) RT-qPCR of *RNAIII* in PAPA/NO-treated *S. aureus* cultures (n=3) chromosomally expressing an AgrC allele with two site-specific mutations (C91S and C371S).

For (A) through (F) data are represented as means with error bars showing standard deviation.

See also Figure S2.

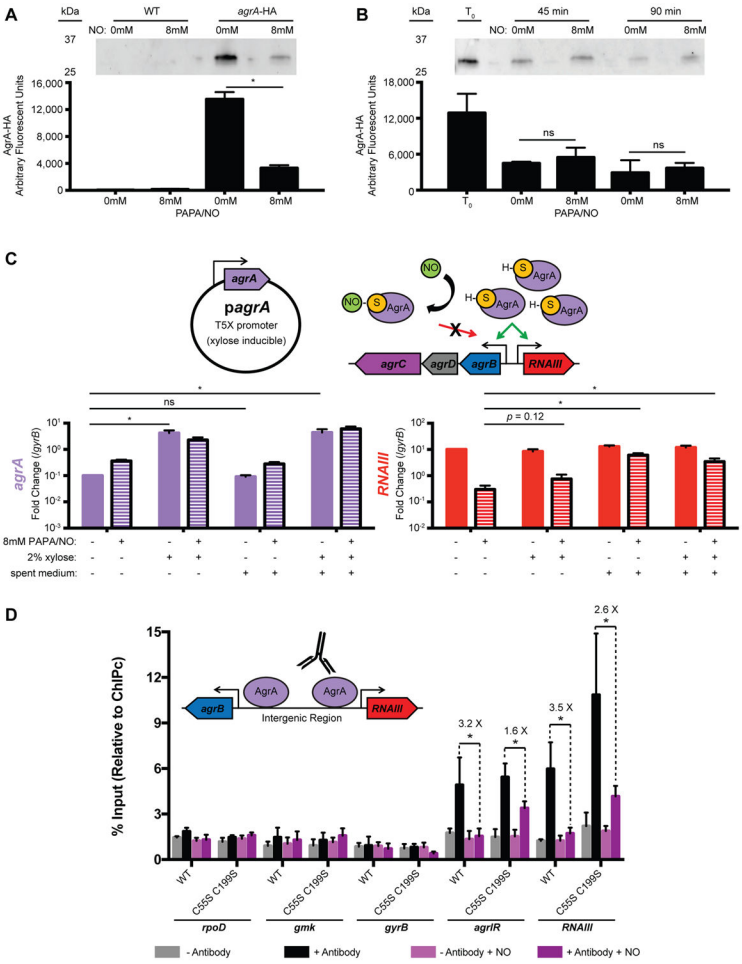

Figure 4. *S*-nitrosylation of AgrA Disrupts Agr Auto-Activation by Decreasing AgrA Occupancy at Target Promoters

(A) Western blot of HA-tagged AgrA from *S. aureus* cultures treated with NO (n=3).

(B) Western blot of HA-tagged AgrA from *S. aureus* cultures treated with NO after inhibition of protein synthesis with tetracycline (n=2).

(C) RT-qPCR of *agrA* and RNAIII from cultures ectopically expressing AgrA and activated with spent medium preceding NO treatment (n=3).

(D) ChIP-qPCR of NO treated *S. aureus* wild-type and *agrA* C55S C199S cultures (n=3). DNA regions proximal to AgrA binding sites include *agrIR* and *RNAIII*; control regions include *rpoD*, *gmk*, and *gyrB.* All chromosomal regions are normalized to the *ChIPc* control region located several kilobases away from *agr* intergenic region. The numbers above bars indicate fold difference between the means of indicated samples. The *p* values comparing the NO-dependent differences (untreated vs. NO-treated) between WT and *agrA* C55S C199S are 0.045 for *agrIR* and 0.25 for RNAIII.

Student's t test, **p*<0.05; ns, not significant.

For (A) through (D) data are represented as means with error bars showing standard deviation..

See also Figure S3.

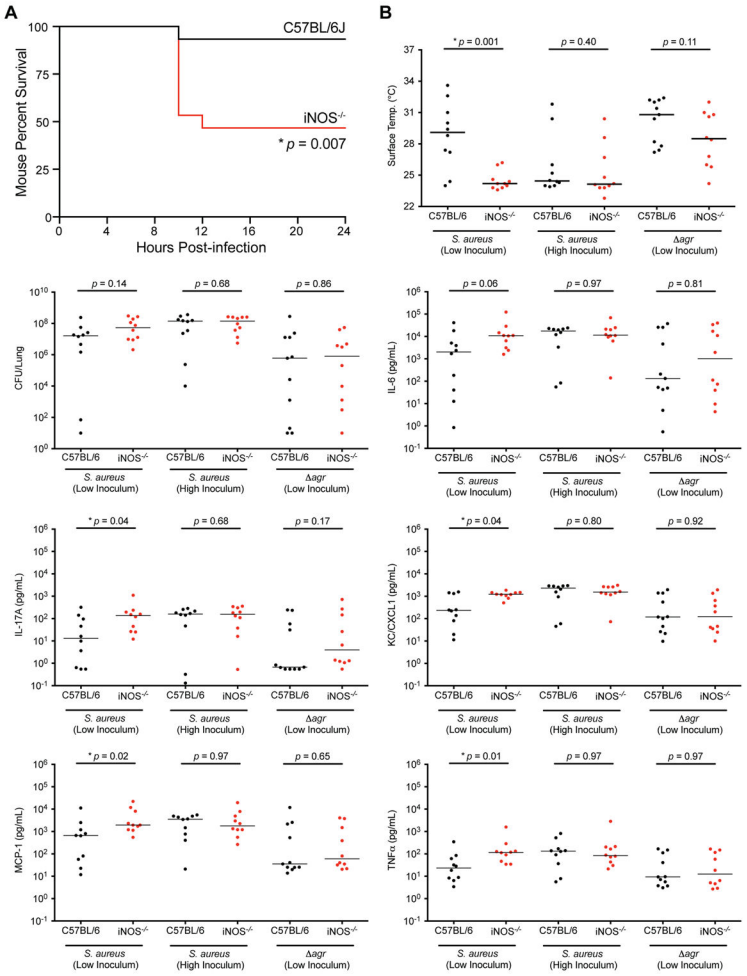

Figure 5. Nitric Oxide is Protective in Staphylococcal Pneumonia

(A) Mouse percent mortality of C57BL/6 (black line, n=15) and congenic iNOS$^{-/-}$ (red line, n=15) mice at indicated time points post-infection with *S. aureus* Newman (~5 × 10^7 CFU). Kaplan-Meier plot, *p<0.05.

(B) Mouse body surface temperature, bacterial burden (CFU per lung), and pro-inflammatory cytokines levels of C57BL/6 (black circles, n=10) and congenic iNOS$^{-/-}$ (red circles, n=10) mice measured at 8 h post-infection. Two inocula are indicated for infections with wild-type *S. aureus* (~5 × 10^7 or ~1 X 10^8 CFU) and one inoculum for mice infected with an *agr* mutant (~5 × 10^7 CFU).

Individual values are plotted with horizontal lines showing medians of groups, Mann-Whitney U test, *p<0.05.

See also Figure S4–S5.

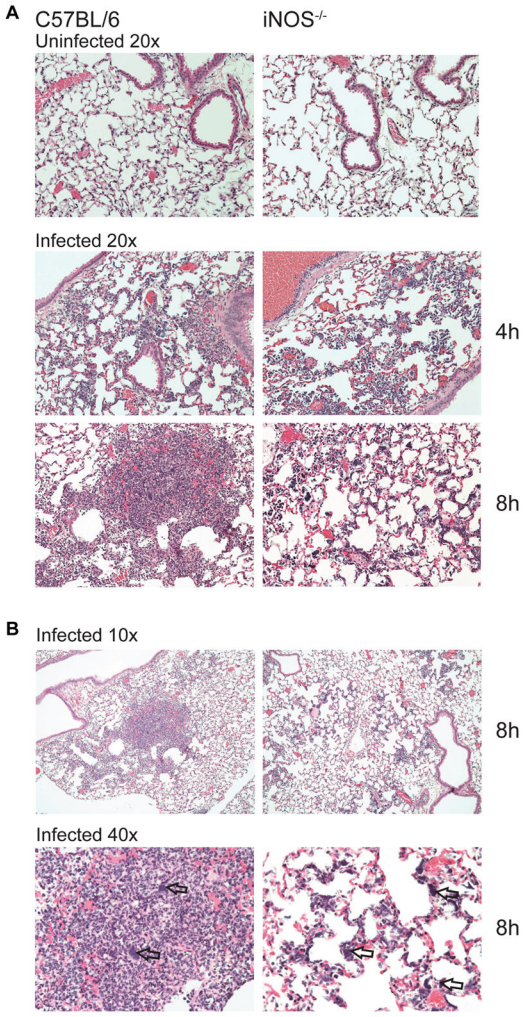

Figure 6. Deficiency in Host Nitric Oxide Production Alters the Histopathological Pattern of Staphylococcal Pneumonia

(A) Representative H&E stains of lung section at 20x magnification from C57BL/6 and iNOS knockout male mice either uninfected (top panels) or infected with ~1 × 10^8 CFU at 4 h (middle panel) and 8 h (bottom panel) post-infection.

(B) Representative H&E stains of lung sections at 10x (top panel) and 40x (bottom) magnification from C57BL/6 and iNOS knockout male mice at 8 h post-infection. Arrows indicate bacterial clusters.

See also Figure S6 and Table S2.

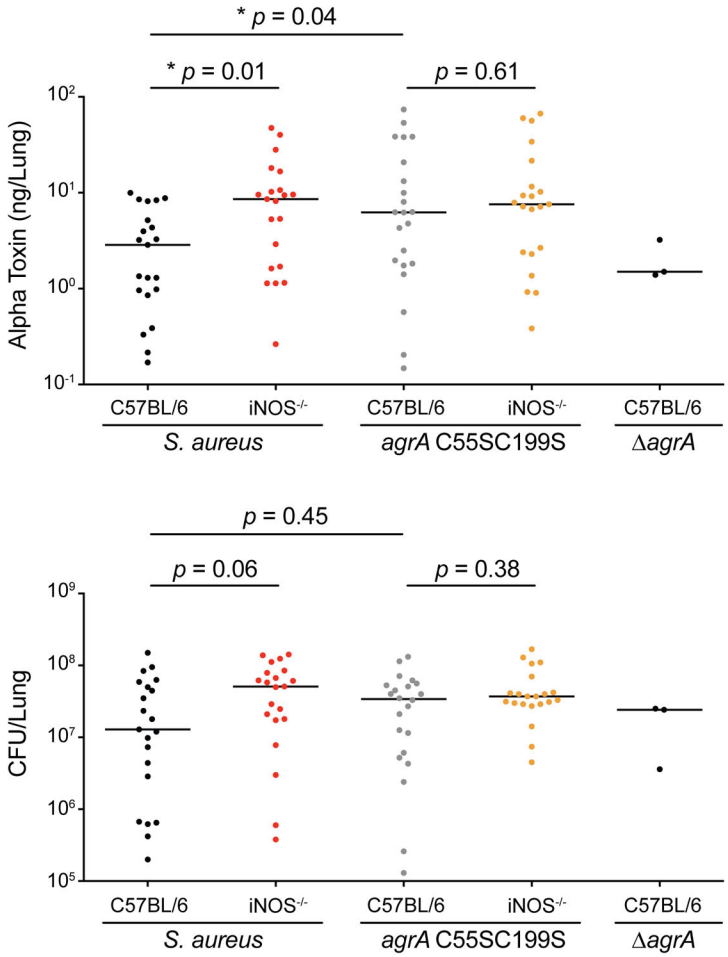

Figure 7. Alpha-Toxin Production Is Higher in iNOS-Deficient Mice and Dependent on AgrA Cysteine Residues during Staphylococcal Pneumonia

Alpha-toxin levels in mouse lungs (top) and bacterial burden (bottom) at 8h post-infection. Mice were infected with ~5 × 10^7 CFU of wild-type *S. aureus* Newman, *agrA* C55S C199S (nitric oxide-resistant mutant), or *ΔagrA* (null). Alpha-toxin measurements were determined on lung homogenates by ELISA.

Individual values are plotted with horizontal lines showing medians of groups, Mann-Whitney U test, *p<0.05 (n = 20).

See also Figure S7.